Supporting Information

Pharmaceutical targeting of OTUB2 sensitizes tumors to cytotoxic T cells via degradation of PD-L1

Wenfeng Ren[1†], Zilong Xu[1†], Yating Chang[1,2†], Fei Ju[1†], Hongning Wu[1,2†], Zhiqi Liang[1,2†], Min Zhao[1], Naizhen Wang[1], Yanhua Lin[1], Chenhang Xu[1,2], Shengming Chen[1], Yipeng Rao[1], Chaolong Lin[1,3], Jianxin Yang[4,5], Pingguo Liu[4,5*], Jun Zhang[1,3*], Chenghao Huang[1,3*], Ningshao Xia[1,2,3*]

[1]State Key Laboratory of Molecular Vaccinology and Molecular Diagnostics, National Institute of Diagnostics and Vaccine Development in Infectious Diseases, Department of Laboratory Medicine, School of Public Health, Xiamen University, Xiamen, Fujian, China, 361102
[2]School of Life Sciences, Xiamen University, Xiamen, Fujian, China, 361102
[3]Xiang An Biomedicine Laboratory, Xiamen, Fujian China, 361102
[4]Department of Hepatobiliary & Pancreatic Surgery, The National Key Clinical Specialty, Zhongshan Hospital of Xiamen University, School of Medicine, Xiamen University, Xiamen, Fujian, China, 361004
[5]Fujian Provincial Key Laboratory and Chronic Liver Disease and Hepatocellular Carcinoma, Xiamen, Fujian, China, 361004
†These authors contributed equally: Wenfeng Ren, Zilong Xu, Yating Chang, Fei Ju, Hongning Wu and Zhiqi Liang.
*Corresponding authors: nsxia@xmu.edu.cn; huangchenghao@xmu.edu.cn; zhangj@xmu.edu.cn; pgliu@xmu.edu.cn.

Inventory of Supporting Information

Supplementary Fig. 1

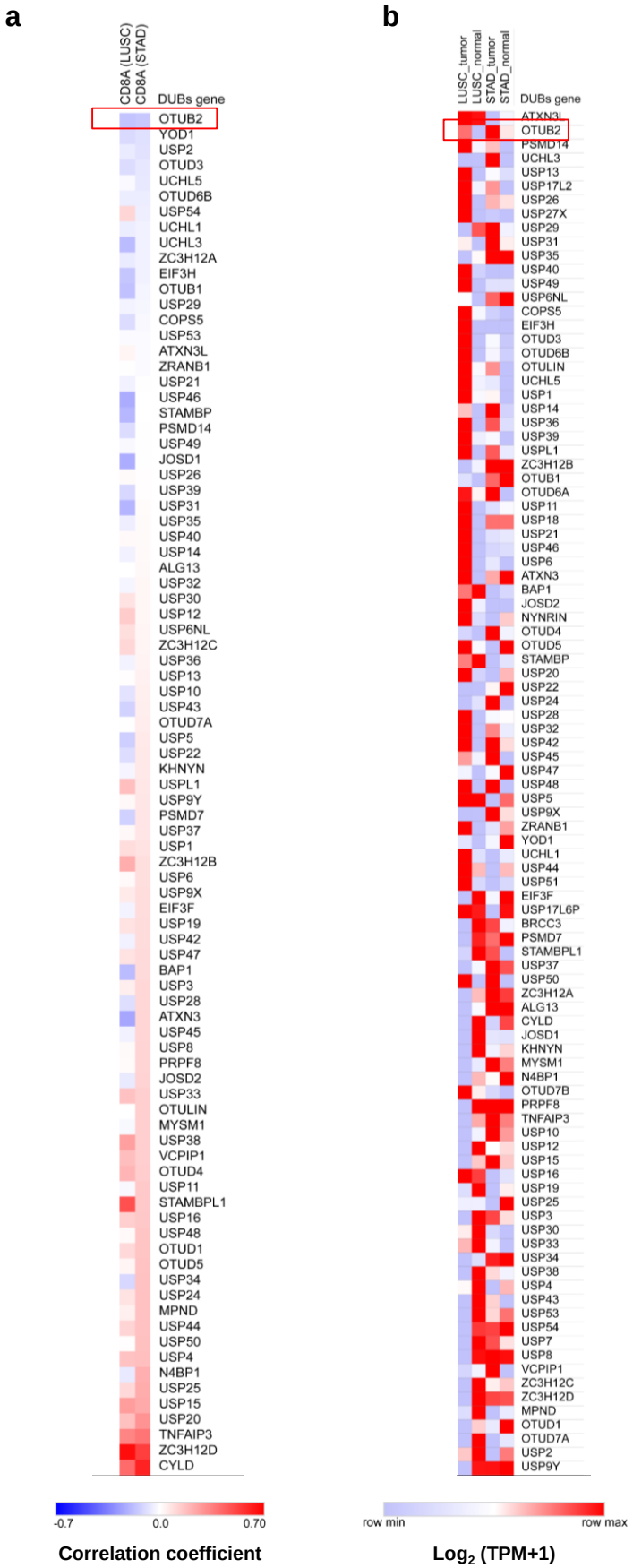

Supplementary Fig. 1. Bioinformatic analyses identifies OTUB2 as a negative regulator in the TME. a, Pearson's correlation coefficients between *CD8A* and 103 DUBs using the indicated datasets from TCGA database. **b,** Heatmap visualization of the gene expression levels of OTUB2 in different cancer tissues (Tumor) and adjacent paracancerous tissues (Normal) in the indicated datasets from TCGA database. Data are shown as $\log_2$ (TPM+1). TPM, transcripts per million. Expression data of USP52, HAUSP, PPPDE1 and CSN6 are not available in the indicated datasets.

Supplementary Fig. 2

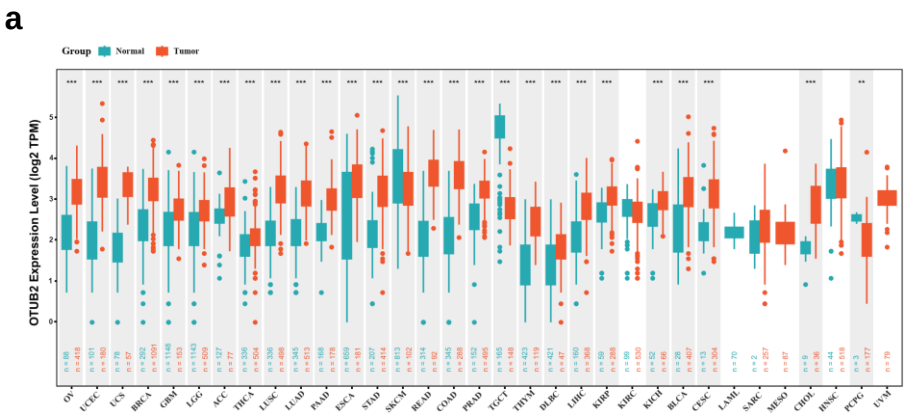

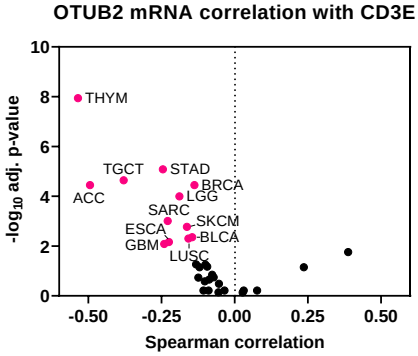

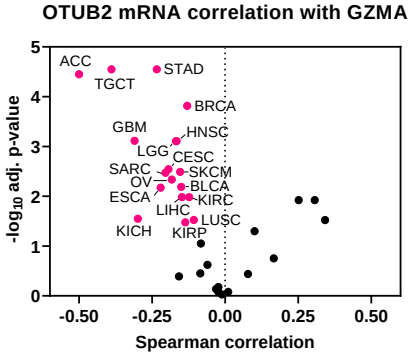

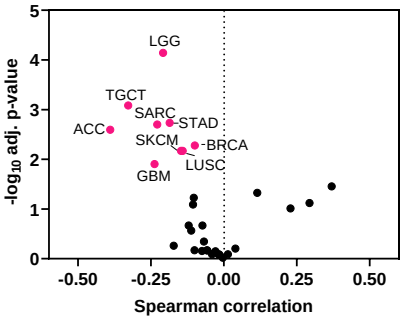

Supplementary Fig. 2. Pancancer dissection of the transcriptomic signature of CD8$^+$ T-cell-associated genes associated with OTUB2 expression in the TCGA database. a, Differential expression of *OTUB2* across tumor samples for all cancer types compared with normal samples. Analyses were performed using data from TCGA datasets. Cancer types with significant upregulation of *OTUB2* are labeled in gray. **b,** Volcano plot of the Spearman correlation between *OTUB2* and *CD3E* mRNA expression in 31 cancer types. Data from the TCGA database were analyzed. Magenta points indicate cancer types in which *OTUB2* was significantly negatively correlated with *CD3E* (adjusted $P < 0.05$). **c,** Volcano plot of the Spearman correlation between *OTUB2* and *GZMA* mRNA expression in 32 cancer types. Data from the TCGA database were analyzed. Magenta points indicate cancer types in which *OTUB2* was significantly negatively correlated with *GZMA* (adjusted $P < 0.05$). **d,** Volcano plot of the Spearman correlation between *OTUB2* and *CD69* mRNA expression in 32 cancer types. Magenta points indicate cancer types in which *OTUB2* was significantly negatively correlated with *CD69* (adjusted $P < 0.05$). The data are presented as the mean ± s.e.m., and P values were calculated using the Spearman's correlation test (**b**-**d**) except for in **a,** in which P values were calculated by an unpaired two-sided Student's t test. $^{**}P < 0.01$; $^{***}P < 0.001$.

Supplementary Fig. 3

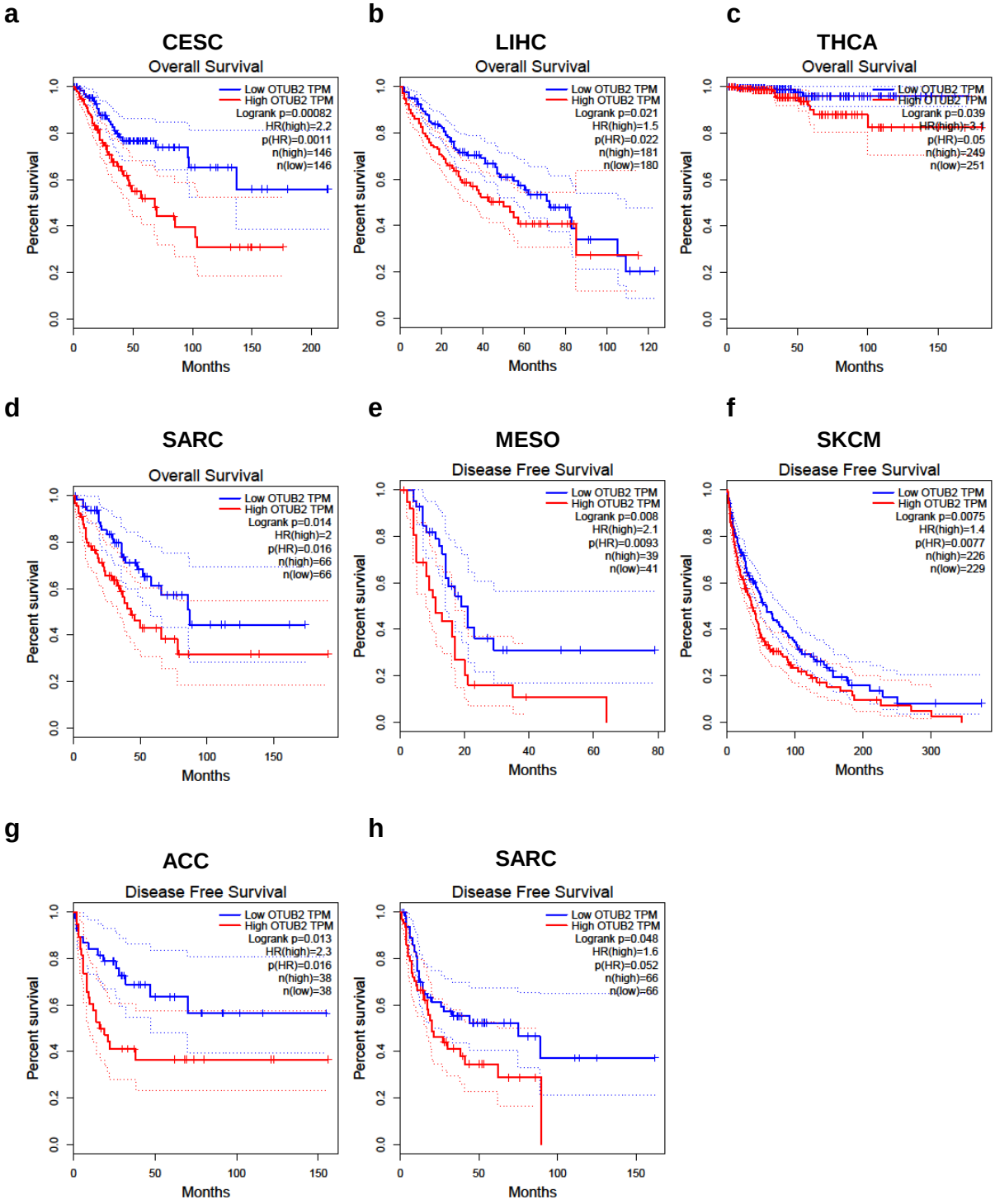

Supplementary Fig. 3. Associations between OTUB2 expression and the survival of patients in the TCGA database. a-d, Overall survival of CESC patients (**a**), LIHC patients (**b**), THCA patients (**c**) and SARC patients (**d**) grouped based on OTUB2 expression; data from the TCGA database were analyzed. **e-h,** Disease-free survival of MESO patients (**e**), SKCM patients (**f**), ACC patients (**g**) and SARC patients (**h**) grouped based on OTUB2 expression; data from the TCGA database were analyzed. The data are presented as the mean ± s.e.m., and P values were calculated by the log-rank test (**a**-**h**).

Supplementary Fig. 4

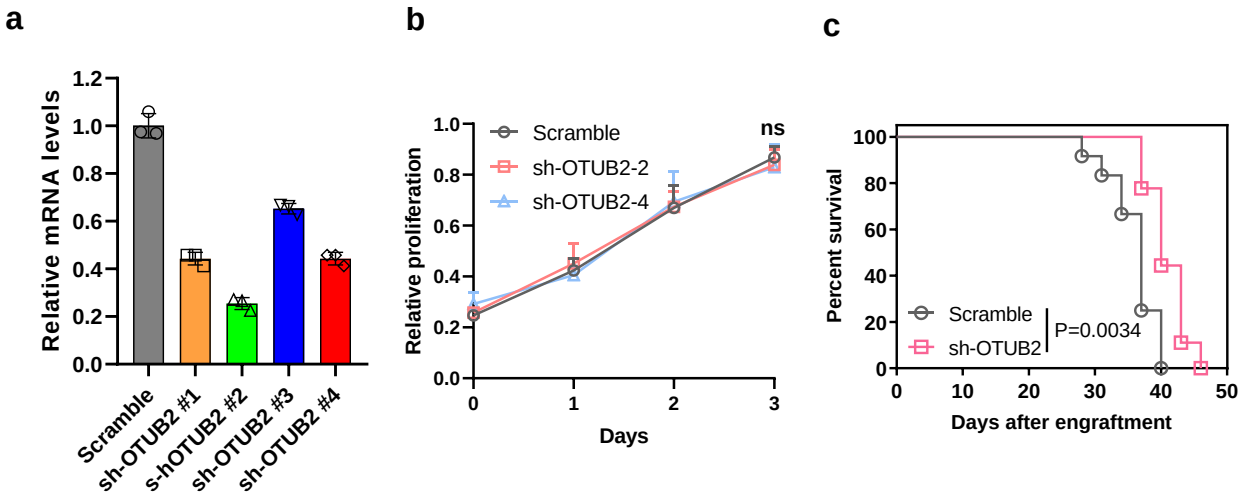

Supplementary Fig. 4. Effects of OTUB2 KD on MC38 tumor-cell growth. a, Knockdown (KD) efficiency of four shRNAs targeting mouse OTUB2. OTUB2 mRNA levels in MC38 tumor cells expressing control shRNA (Scramble) or OTUB2-specific shRNAs (shRNA #1-#4). n = 3 biologically independent experiments. **b,** Vector control (scramble) or OTUB2-KD (sh-OTUB2) MC38 tumor cells were seeded and cell growth was examined using a proliferation assay. n = 3 biologically independent experiments. **c,** Kaplan–Meier survival analysis of host animals bearing vector control or OTUB2-KD MC38 tumors. n = 5 mice per group. The data are presented as the mean ± s.e.m. from at least two independent experiments, and P values were determined by an unpaired two-sided Student's t test (**b**), except for in **c,** in which P values were determined by the log-rank test. ns, not significant.

Supplementary Fig. 5

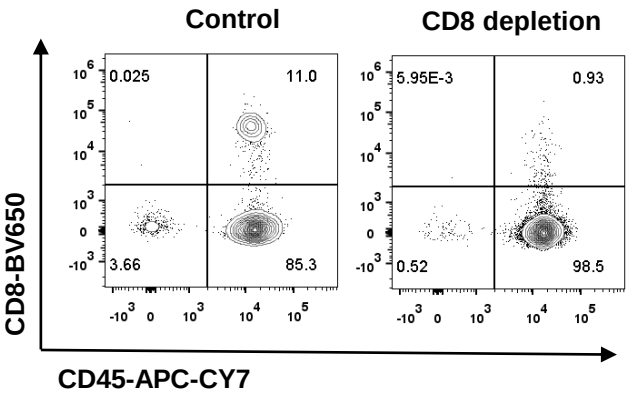

Supplementary Fig. 5. Depletion of $CD8^+$ T cells *in vivo*. Representative plots of $CD8^+$ T-cell depletion from 1 of 3 independent experiments are shown.

Supplementary Fig. 6

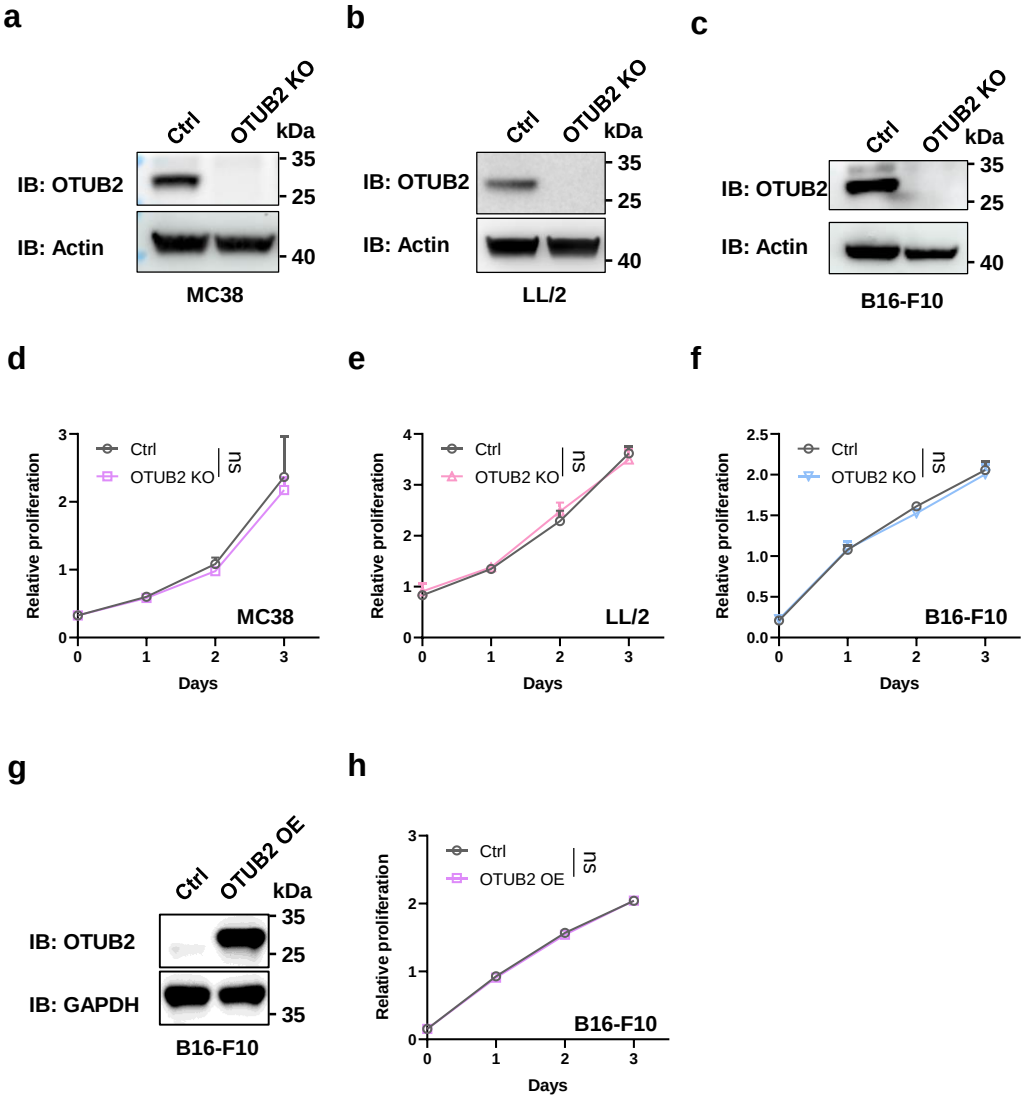

Supplementary Fig. 6. Effects of OTUB2 KO or OE on tumor-cell growth *in vitro*. **a-c,** Western blot analysis of the expression of OTUB2 in murine tumor cell lines (MC38, LL/2 and B16-F10) with or without OTUB2 knockout (OTUB2-KO). Actin was used as a protein loading control. **d-f,** Cell growth of control or OUTB2-KO murine tumor cells (MC38, LL/2 and B16-F10). **g,** Western blot analysis of the expression of OTUB2 in B16-F10 tumor cell lines overexpressing OTUB2 (OTUB2-OE). GAPDH was used as a protein loading control. **h,** Cell growth of control or OUTB2-OE B16-F10 tumor cells. The data are presented as the mean ± s.e.m. from three independent experiments (n = 3), and P values were calculated using two-way analysis of variance (ANOVA). Source data are provided as a Source Data file. ns, not significant.

Supplementary Fig. 7

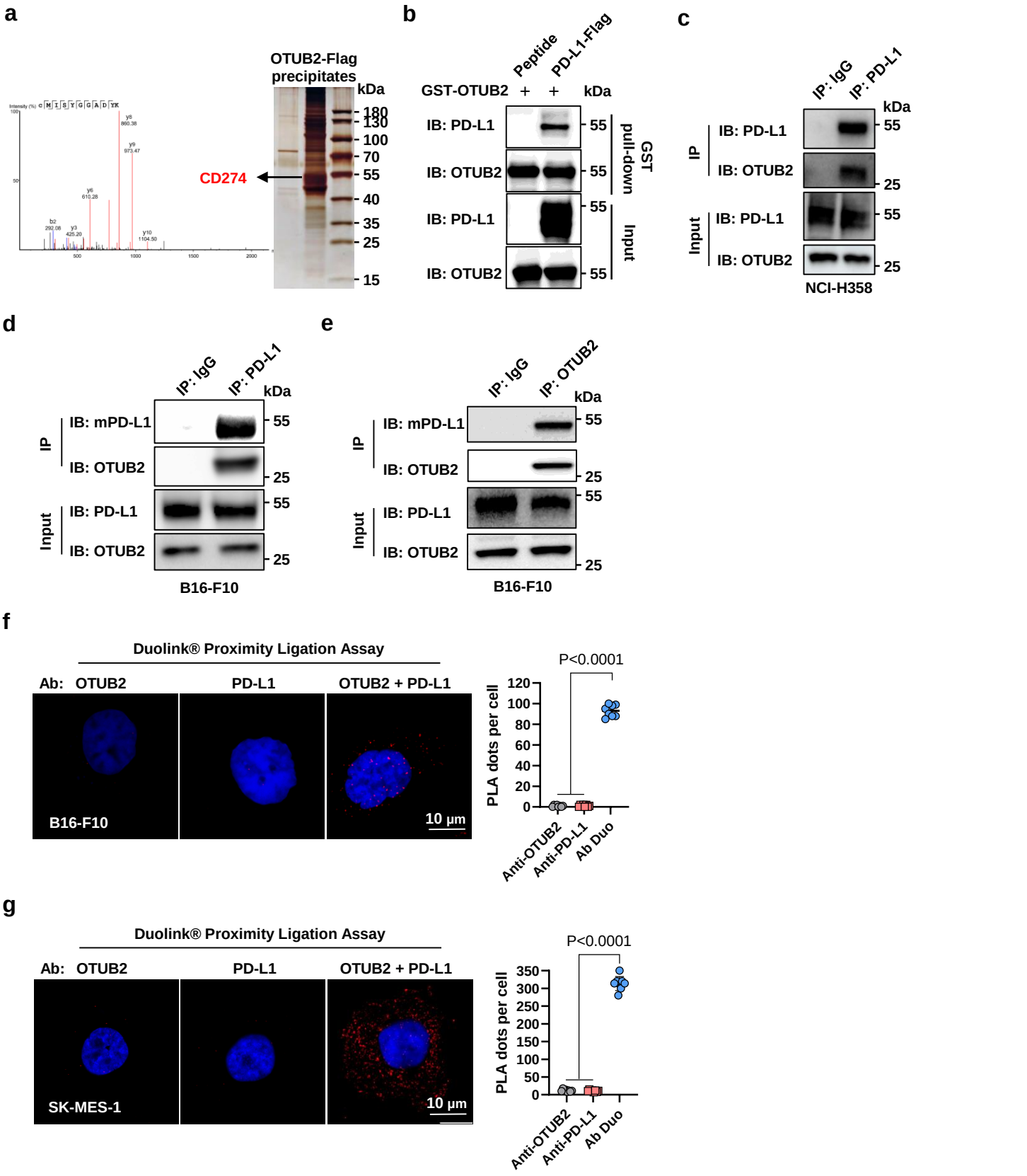

Supplementary Fig. 7. OTUB2 interacts with PD-L1 in B16-F10 and SK-MES-1 cells. a, Silver staining of OTUB2-Flag precipitates from B16-F10 cells. **b,** The *in vitro* interaction between purified PD-L1-Flag proteins and GST-OTUB2 proteins examined by *in vitro* GST pull-down assays. **c,** Immunoprecipitation was performed with an anti-PD-L1 antibody to examine the interaction between endogenous OTUB2 and PD-L1 in NCI-H358 cells. **d,** Immunoprecipitation was performed with an anti-PD-L1 antibody to examine the interaction between endogenous OTUB2 and PD-L1 in B16-F10 cells. **e,** Immunoprecipitation was performed with an anti-OTUB2 antibody to examine the interaction between endogenous OTUB2 and PD-L1 in B16-F10 cells. **f,g,** *In situ* interaction between OTUB2 and PD-L1 in B16-F10 (**f**) and SK-MES-1 (**g**) cells. After fixation, a Duolink *in situ* PLA was performed with anti-OTUB2 and anti-PD-L1 antibodies to assess the OTUB2-PD-L1 interaction. Quantification of the PLA dots indicating PD-L1-OTUB2 interactions is shown as the mean ± s.e.m.. Scale bar, 10 μm. n = 8 biologically independent samples. The data are presented as the mean ± s.e.m., and P values were calculated using an unpaired two-sided Student's t test (**f** and **g**). Source data are provided as a Source Data file.

Supplementary Fig. 8

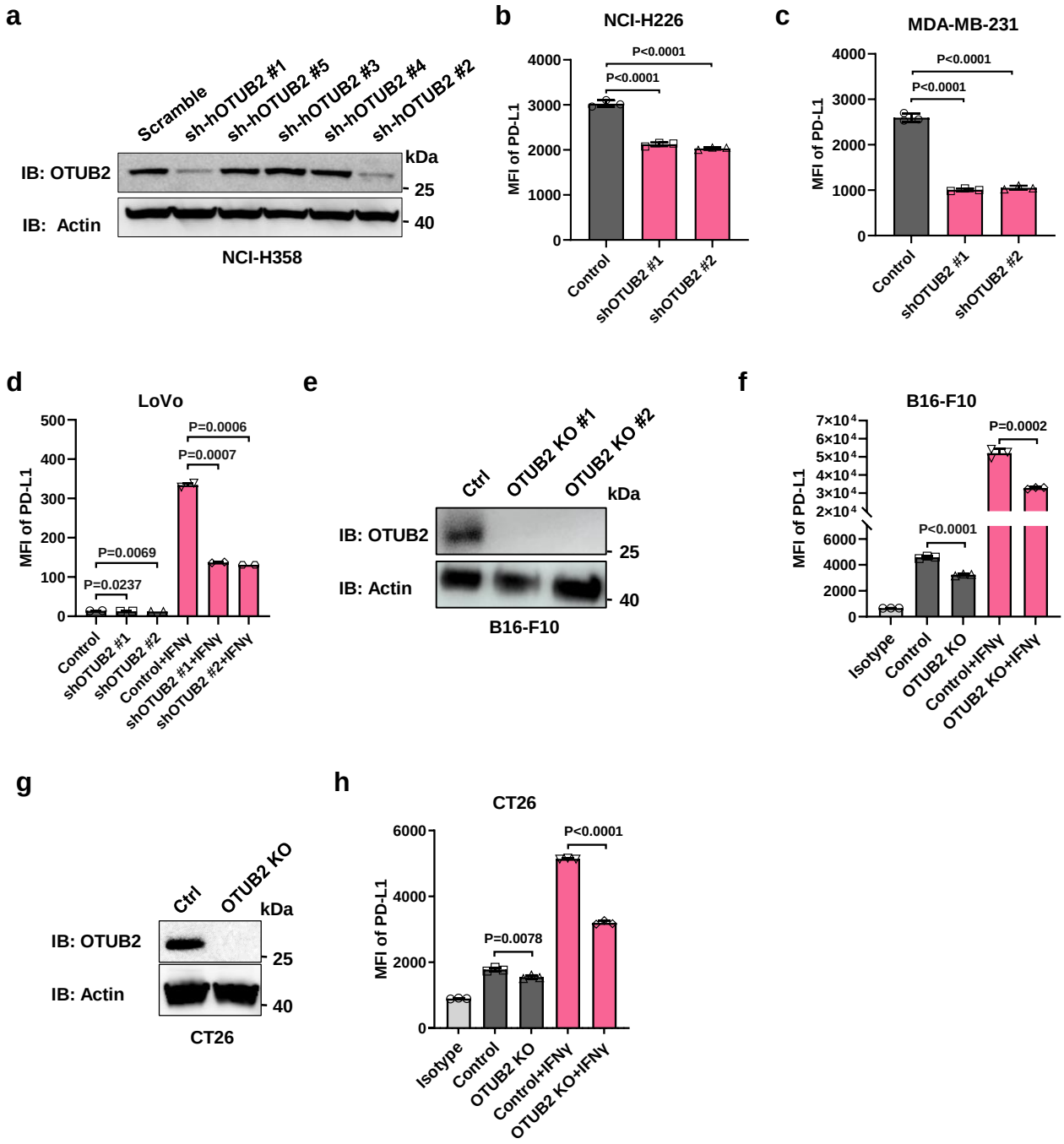

Supplementary Fig. 8. Effects of OTUB2 KD or KO on the expression of PD-L1. **a,** Knockdown (KD) efficiency of five shRNAs targeting human OTUB2. OTUB2 protein levels in NCI-H358 tumor cells expressing control shRNA (Scramble) or OTUB2-specific shRNAs (shRNA #1-#5). **b,** Flow cytometry analysis of PD-L1 levels on the surface of control and OTUB2-KD NCI-H226 cells. MFI, median fluorescence intensity. n = 3 biologically independent experiments. **c,** Flow cytometry analysis of PD-L1 levels on the surface of control and OTUB2-KD MDA-MB-231 cells. n = 3 biologically independent experiments. **d,** Flow cytometry analysis of PD-L1 levels on the surface of control and OTUB2-KD LoVo cells treated with or without IFN-γ. n = 2 biologically independent experiments. **e,** Western blot analysis of two independent OTUB2-KO B16-F10 clones (OTUB2 KO #1 and #2). **f,** Flow cytometry analysis of PD-L1 levels on the surface of control and OTUB2-KO B16-F10 cells treated with or without IFN-γ. n = 3 biologically independent experiments. **g,** Western blot analysis of the expression of OTUB2 in CT26 tumor cell lines with and without OTUB2 KO. **h,** Flow cytometry analysis of PD-L1 levels on the surface of control and OTUB2-KO CT26 cells treated with or without IFN-γ. n = 3 biologically independent experiments. The experiments were repeated three times independently with similar results. The data are presented as mean ± s.e.m., and P values were calculated using an unpaired two-sided Student's t test (**b**,**c**,**d**,**f**,**h**). Source data are provided as a Source Data file.

Supplementary Fig. 9

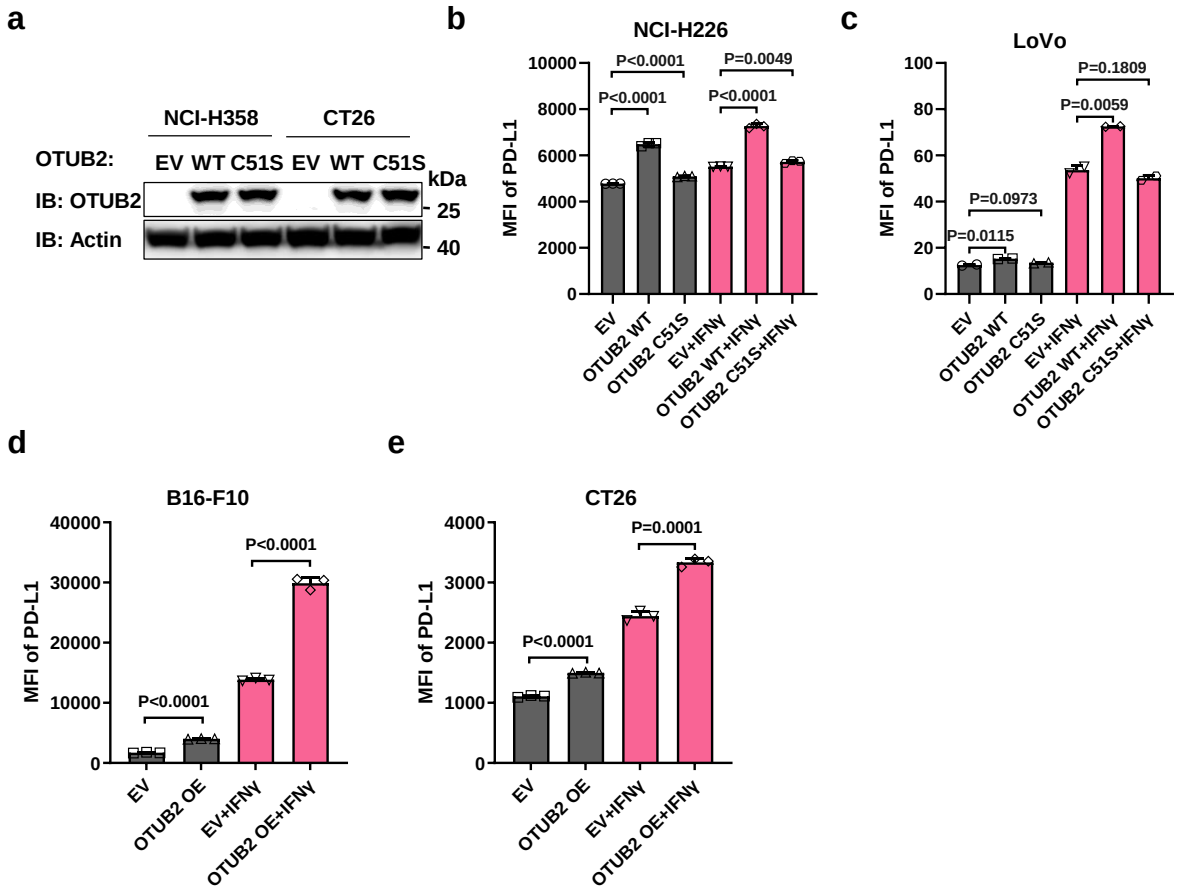

Supplementary Fig. 9. Effects of OTUB2 OE on the expression of PD-L1. a, Western blot analysis of the expression of OTUB2-WT and C51S in NCI-H358 and CT26 tumor cell lines. **b,** Flow cytometry analysis of PD-L1 levels on the surface of control and OTUB2-OE NCI-H226 cells treated with or without IFN-γ. MFI, median fluorescence intensity. n = 3 biologically independent experiments. **c,** Flow cytometry analysis of PD-L1 levels on the surface of control and OTUB2-OE LoVo cells treated with or without IFN-γ. n = 2 biologically independent experiments. **d,** Flow cytometry analysis of PD-L1 levels on the surface of control and OTUB2-OE B16-F10 cells treated with or without IFN-γ. n = 3 biologically independent experiments. **e,** Flow cytometry analysis of PD-L1 levels on the surface of control and OTUB2-OE CT26 cells treated with or without IFN-γ. n = 3 biologically independent experiments. The experiments were repeated three times independently with similar results. The data are presented as mean ± s.e.m., and P values were calculated using an unpaired two-sided Student's t test (**b**-**e**). Source data are provided as a Source Data file.

Supplementary Fig. 10

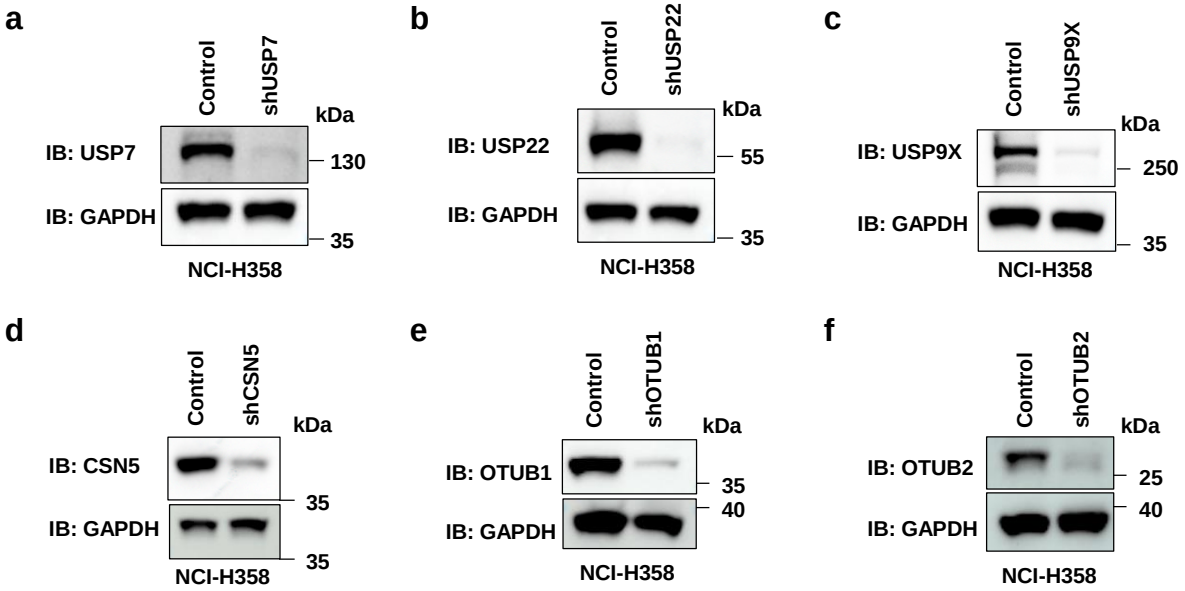

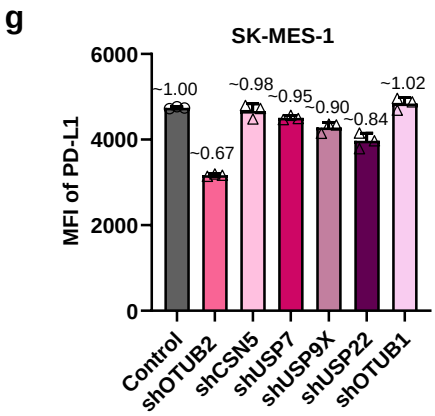

Supplementary Fig. 10. Knockdown (KD) efficiency of shRNAs targeting different DUBs. a, USP7 protein levels in NCI-H358 tumor cells expressing control shRNA or a USP7-specific shRNA. **b,** USP22 protein levels in NCI-H358 tumor cells expressing control shRNA or a USP22-specific shRNA. **c,** USP9X protein levels in NCI-H358 tumor cells expressing control shRNA or a USP9X-specific shRNA. **d,** CSN5 protein levels in NCI-H358 tumor cells expressing control shRNA or a CSN5-specific shRNA. **e,** OTUB1 protein levels in NCI-H358 tumor cells expressing control shRNA or an OTUB1-specific shRNA. **f,** OTUB2 protein levels in NCI-H358 tumor cells expressing control shRNA or an OTUB2-specific shRNA. **g,** Screening of other five DUBs that regulate PD-L1 protein level. SK-MES-1 cells individually were infected with shRNAs targeting different DUBs, and the surface expression of PD-L1 was detected. Each value above the bar is expressed as a fold change relative to the control. n = 3 biologically independent experiments. The experiments were repeated twice independently with similar results. Source data are provided as a Source Data file.

Supplementary Fig. 11

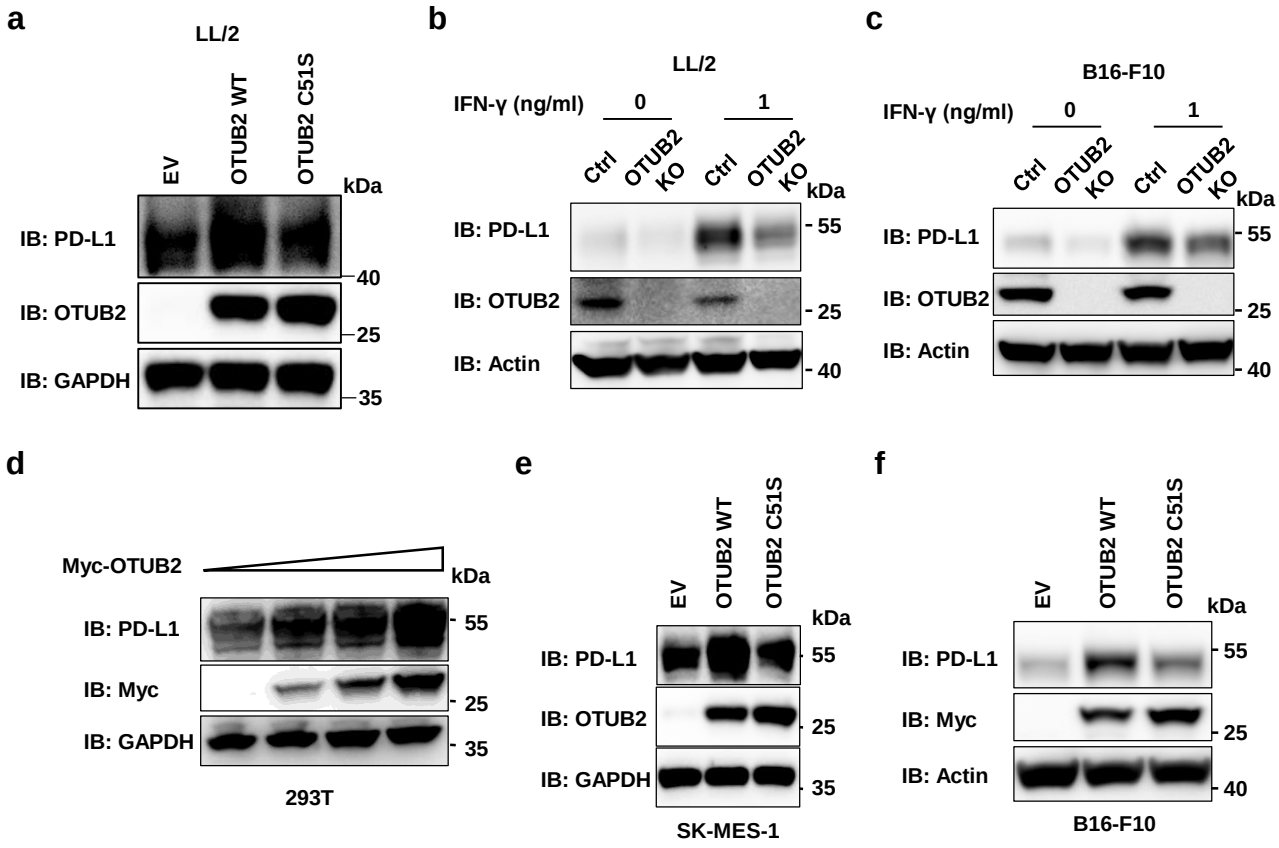

Supplementary Fig. 11. Effects of OTUB2 OE or KO on the expression of PD-L1. **a,** Western blot analysis of PD-L1 in LL/2 cells overexpressing a control vector (EV), OTUB2 (WT) or the OTUB2 C51S mutant (C51S). **b,** Western blot analysis of PD-L1 in control and OTUB2-KO LL/2 cells treated with or without IFN-γ. **c,** Western blot analysis of PD-L1 in control and OTUB2-KO B16-F10 cells treated with or without IFN-γ. **d,** Western blot analysis of endogenous PD-L1 in 293T cells transfected with increasing amounts of OTUB2. **e,** Western blot analysis of PD-L1 in SK-MES-1 cells overexpressing a control vector (EV), OTUB2 (WT) or the OTUB2 C51S mutant (C51S). **f,** Western blot analysis of PD-L1 in B16-F10 cells overexpressing a control vector (EV), OTUB2 (WT) or the OTUB2 C51S mutant (C51S). Source data are provided as a Source Data file.

Supplementary Fig. 12

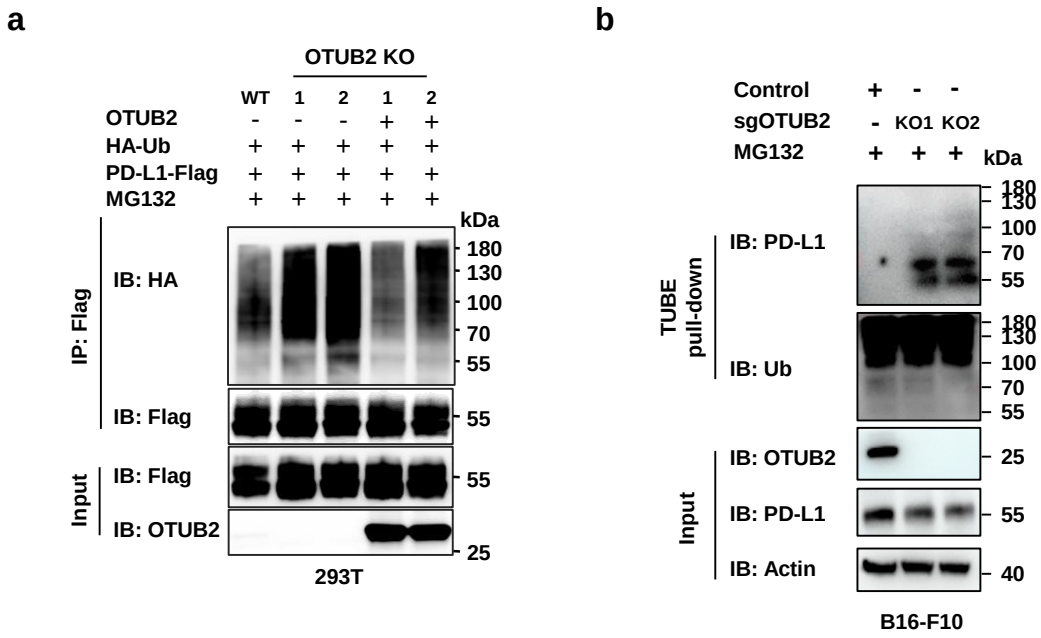

Supplementary Fig. 12. Effects of OTUB2 on the polyubiquitination of PD-L1. a, Determination of PD-L1 polyubiquitination levels in OTUB2-KO 293T cells after re-expression of OTUB2-WT. Immunoprecipitation was performed with an anti-Flag antibody**. b,** Determination of endogenous PD-L1 polyubiquitination levels in OTUB2-KO B16-F10 cells using a TUBE pull-down assay. Source data are provided as a Source Data file.

Supplementary Fig. 13

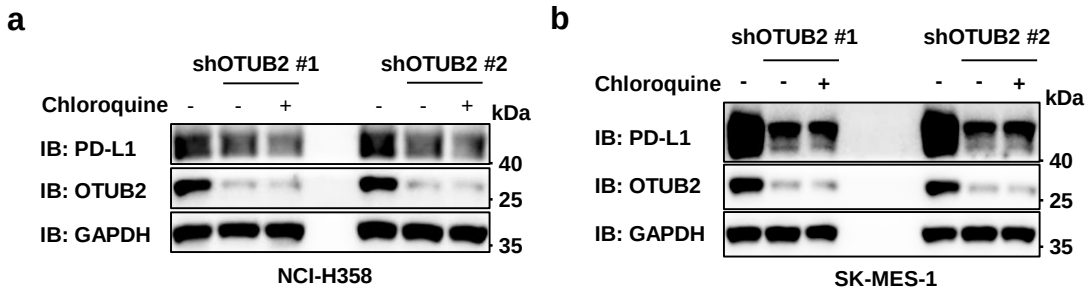

Supplementary Fig. 13. Immunoblot analysis of PD-L1 in lung cancer cells treated with or without the lysosomal inhibitor chloroquine. a, NCI-H358 tumor cells with or without OTUB2 KD in the absence or presence of 20 μM chloroquine (lysosome inhibitor) were collected to analyze PD-L1 expression. **b,** SK-MES-1 tumor cells with or without OTUB2 KD in the absence or presence of 20 μM chloroquine (lysosome inhibitor) were collected to analyze PD-L1 expression. Source data are provided as a Source Data file.

Supplementary Fig. 14

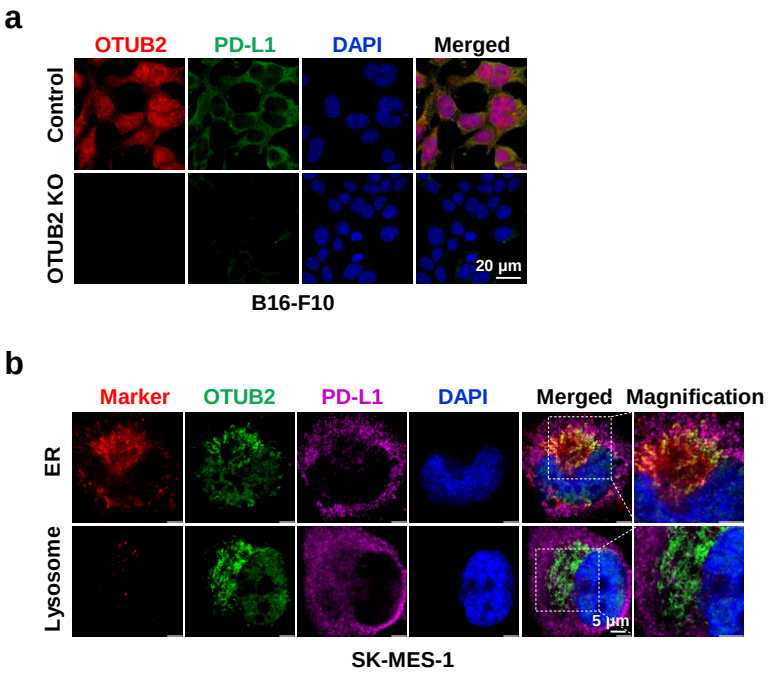

Supplementary Fig. 14. The colocalization of PD-L1 and OTUB2. a, B16-F10 tumor cells with or without OTUB2 KO were immunostained with an anti-OTUB2 antibody (red), an anti-PD-L1 antibody (green), and DAPI (blue). Scale bar, 20 μm. **b,** SK-MES-1 tumor cells were immunostained with an anti-PD-L1 antibody (purple), an anti-OTUB2 antibody (green), DAPI (blue) and lyso- or ER-specific trackers (red). Scale bar, 5 μm.

Supplementary Fig. 15

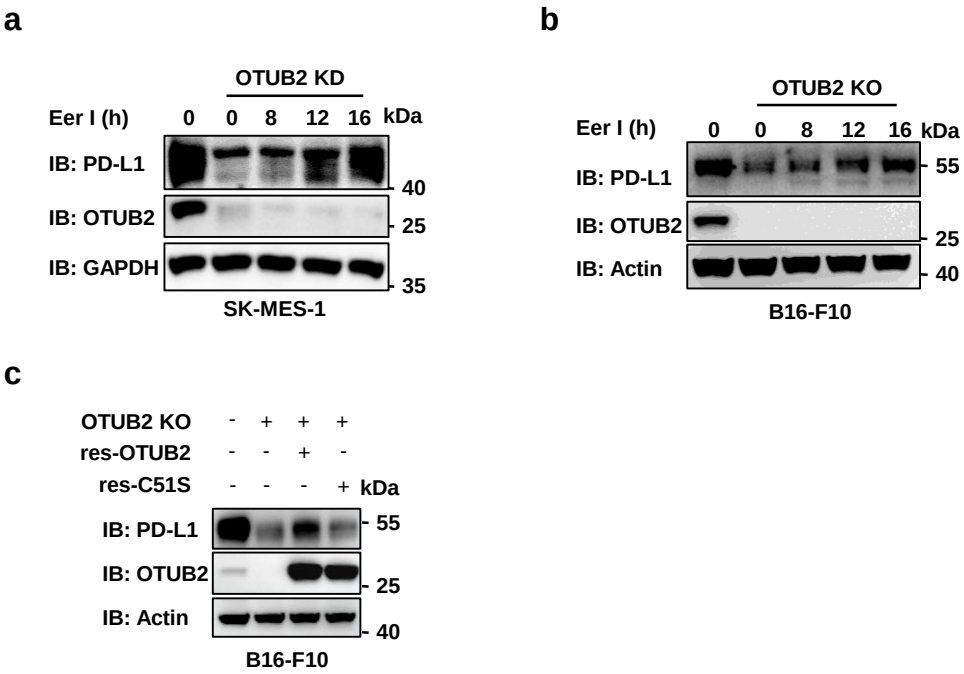

Supplementary Fig. 15. OTUB2 regulates PD-L1 abundance through ERAD pathway. a,b, SK-MES-1 cells (**a**) or B16-F10 tumor cells (**b**) with or without OTUB2 KD/KO in the absence or presence of 20 μM Eer I were collected to analyze PD-L1 expression at the indicated times. **c,** Determination of the PD-L1 levels in OTUB2-KO B16-F10 cells after re-expression of OTUB2-WT or OTUB2-C51S. Source data are provided as a Source Data file.

Supplementary Fig. 16

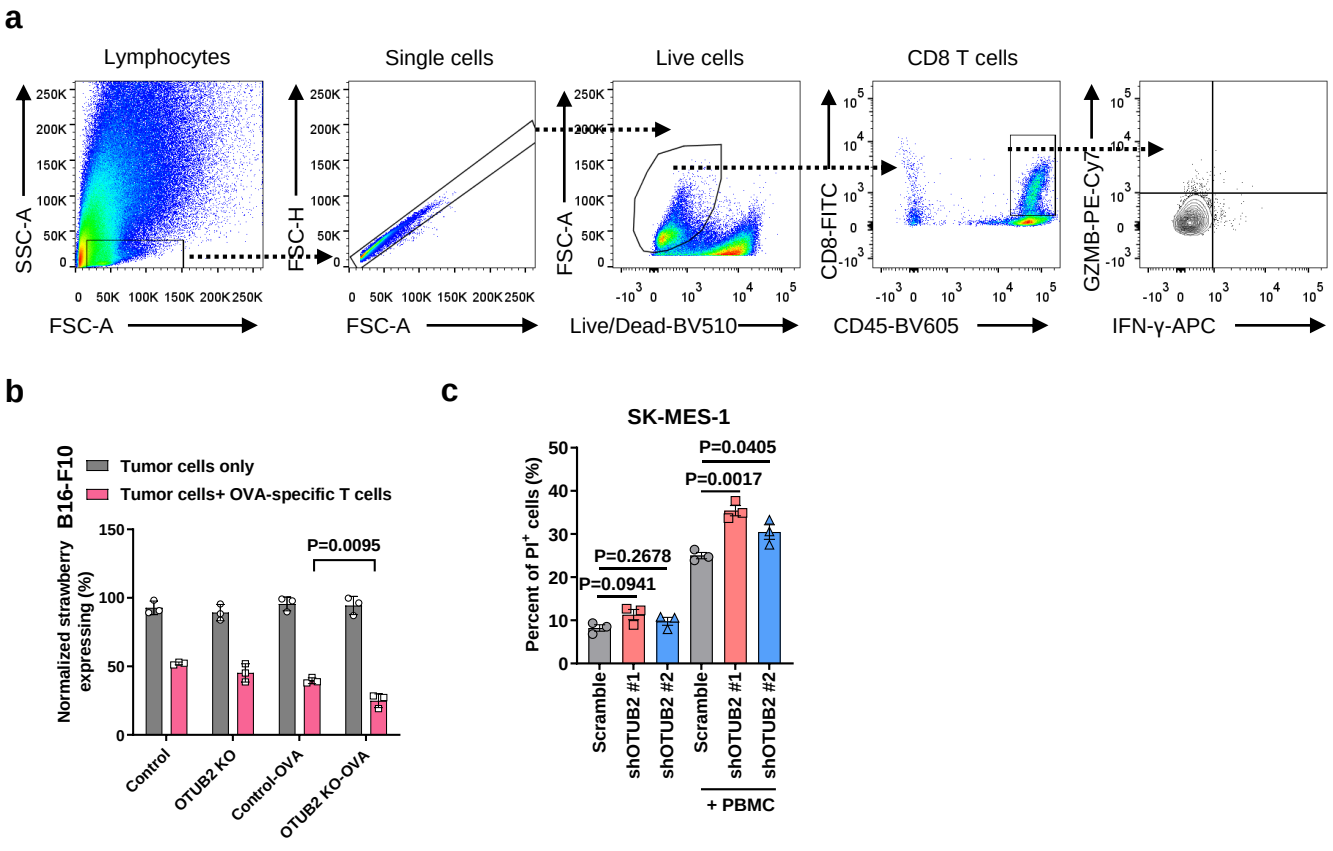

Supplementary Fig. 16. Depletion of OTUB2 enhances intratumoral T-cell infiltration and tumor cell sensitivity to $CD8^+$ T-cell-mediated cytotoxicity. a, Representative flow cytometry gating strategy for quantifying the numbers of various effector immune cell subsets in mouse tumors. **b,** Quantitative estimates of the fractions of live vector control and OTUB2-KO B16-F10-Strawberry tumor cells remaining after 24 h of incubation with activated OVA-specific T cells. **c,** Flow cytometry analysis of the peripheral blood mononuclear cell (PBMC)-mediated killing of vector control or OTUB2-KD SK-MES-1 tumor cells using propidium iodide (PI) staining. n = 3 biologically independent experiments. The above experiments were repeated three times independently with similar results. The data are presented as the mean ± s.e.m., and P values were calculated using an unpaired two-sided Student's t test (**b** and **c**).

Supplementary Fig. 17

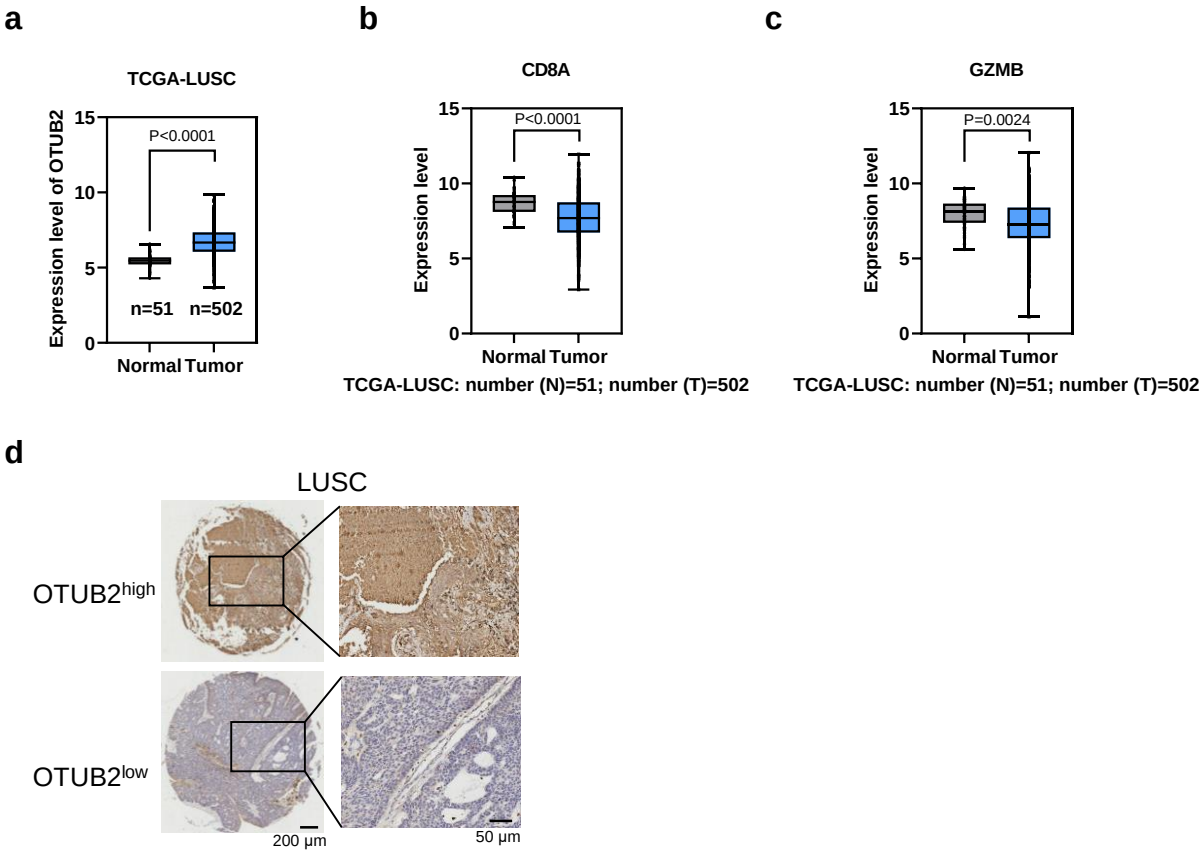

Supplementary Fig. 17. The expression of OTUB2 is positively correlated with PD-L1 abundance. a, Bioinformatic analyses of *OTUB2* mRNA expression in TCGA-LUSC patients (n = 502) relative to that in healthy controls (n = 51). **b,c,** Bioinformatic analyses of *CD8A* (**b**) and *GZMB* (**c**) mRNA expression in TCGA-LUSC patients (n = 502) relative to that in healthy controls (n = 51). **d**, Representative images of IHC staining of LUSC cancer tissues with high or low OTUB2 expression. Scale bars, 200 μm or 50 μm. The data are presented as the mean ± s.e.m., and P values were calculated using an unpaired two-sided Student's t test (**a**-**c**).

Supplementary Fig. 18

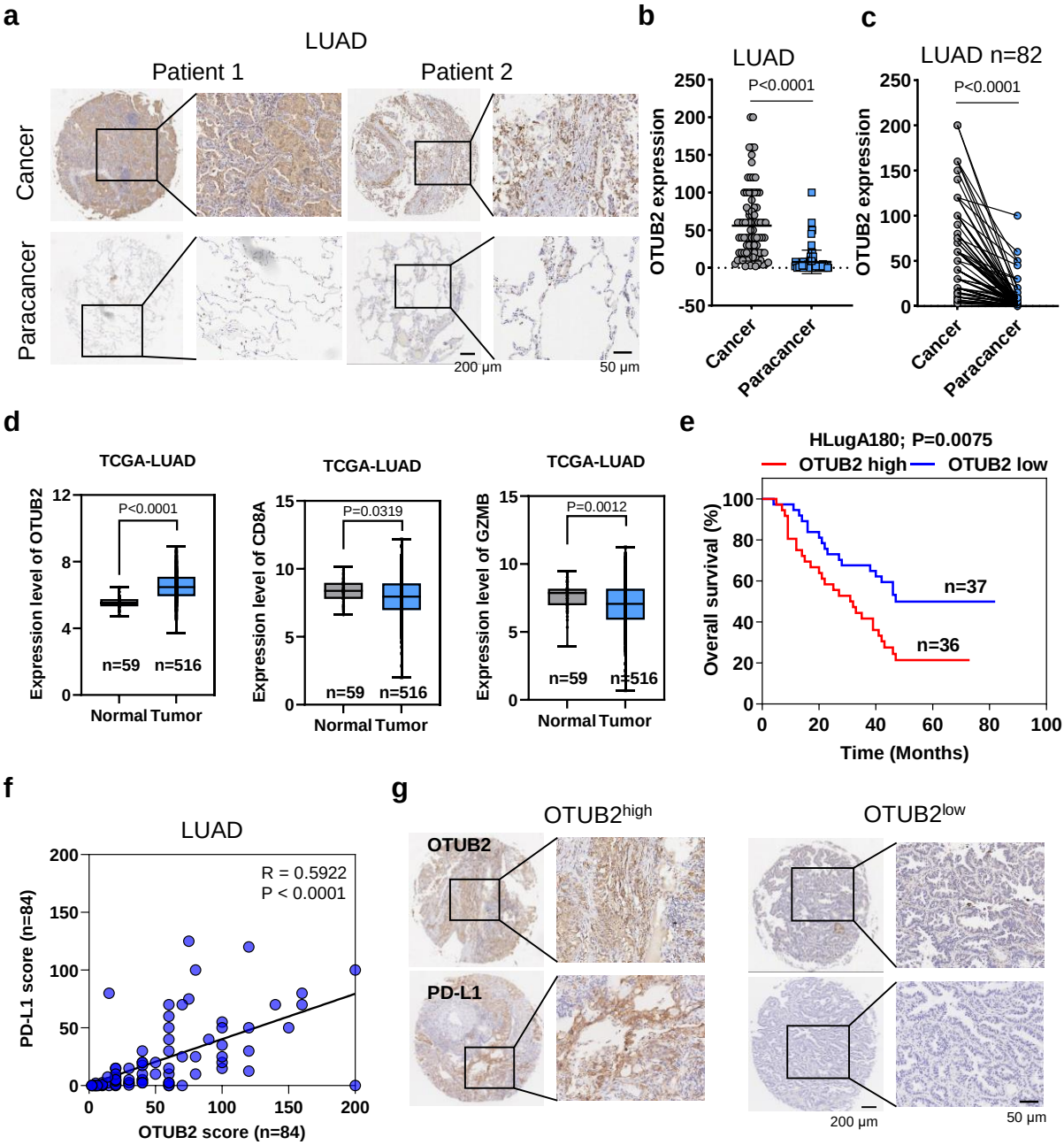

Supplementary Fig. 18. The expression of OTUB2 is positively correlated with PD-L1 abundance in LUAD patient samples. a, Representative images of IHC staining for OTUB2 in cancer tissues and paracancerous tissues from 86 LUAD patients. Scale bars, 200 μm or 50 μm. **b,** Comparison of OTUB2 expression between the cancer tissues (n=82) and paracancerous tissues (n = 82) of LUAD patients. **c,** OTUB2 expression in the paired tissue samples of 82 LUAD patients. **d,** Bioinformatic analyses of OTUB2, CD8A and GZMB expression in TCGA-LUAD patients (n = 516) relative to that in healthy controls (n = 59). **e**, Kaplan–Meier curve for the overall survival of LUAD patients based on OTUB2 expression scores calculated by IHC staining. Patients were divided into a high OTUB2 group (n = 36) or low OTUB1 group (n = 37). **f,** Pearson correlation analysis to determine the association between OTUB2 and PD-L1 by IHC staining scores (n = 84). **g,** Representative images of IHC staining for PD-L1 in LUAD cancer tissues with high or low OTUB2 expression. Scale bars, 200 μm or 50 μm. The data are presented as the mean ± s.e.m., and P values were calculated using an unpaired or paired two-sided Student's t test (**b**-**d**) except for in **e,** in which P values were calculated by the log-rank test, and **f,** in which P values were calculated by Spearman's correlation test.

Supplementary Fig. 19

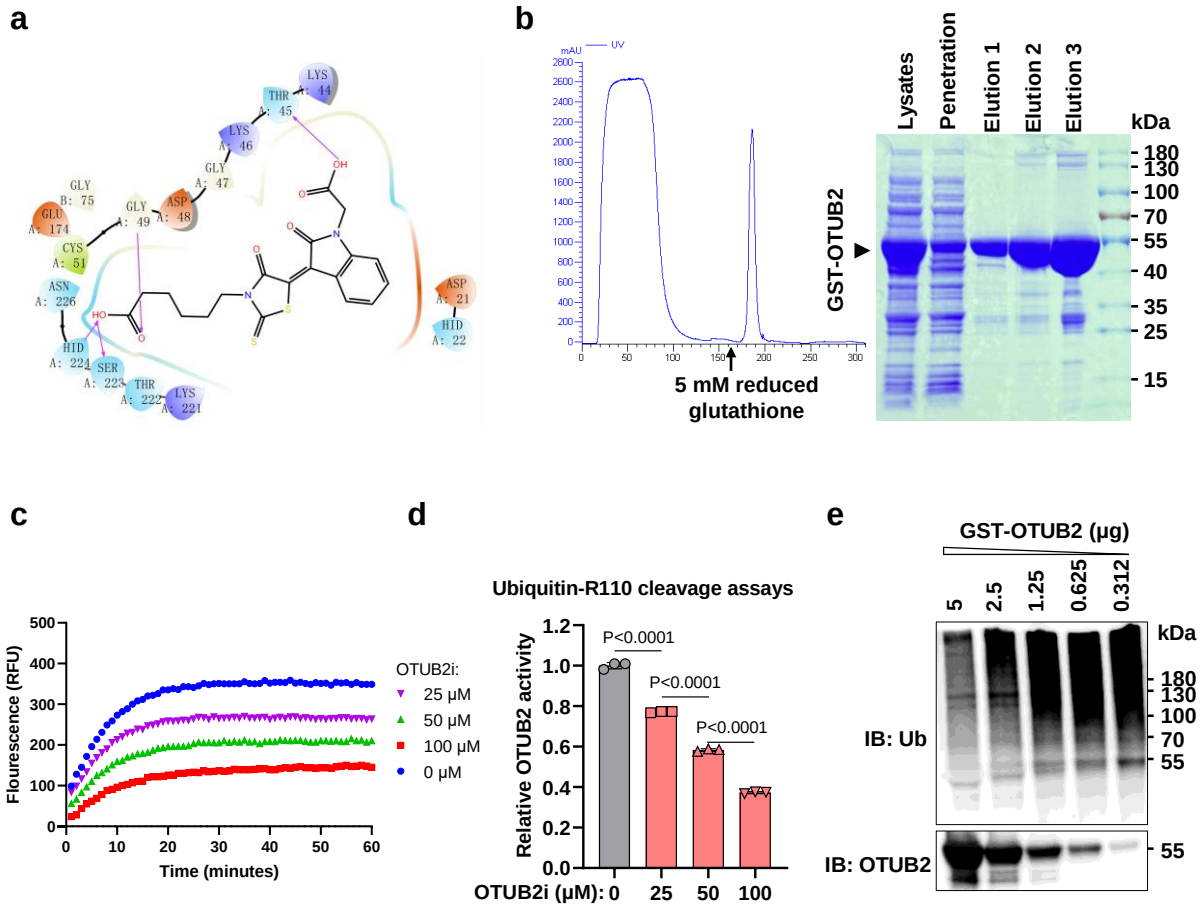

Supplementary Fig. 19. Interaction between OTUB2 and OTUB2-IN-1 and characteristics of prokaryotically expressed GST-OTUB2 proteins. a, A molecular docking model of the compound OTUB2-IN-1 and the catalytic pocket of OTUB2. **b,** Purification of GST-OTUB2 proteins using glutathione-based affinity purification and SDS–PAGE analysis of the purity of the GST-OTUB2 proteins. **c,** Deubiquitinating activity measured by ubiquitin-R110 cleavage assay. Ub-R110 was incubated with GST-OTUB2 in the absence or presence of varying concentrations of OTUB2-IN-1 (OTUB2i) (100, 50 or 25 μM). Deubiquitinating activity was determined by measuring R110 fluorescence as a function of time by fluorescence. **d,** Quantitative estimates of relative OTUB2 activity based on ubiquitin-R110 cleavage. n = 3 biologically independent experiments. **e,** Evaluation of the enzymatic activity of GST-OTUB2 proteins in deubiquitinating PD-L1 *in vitro*. The data are presented as the mean ± s.e.m., and P values were calculated using an unpaired two-sided Student's t test (**d**). Source data are provided as a Source Data file.

Supplementary Fig. 20

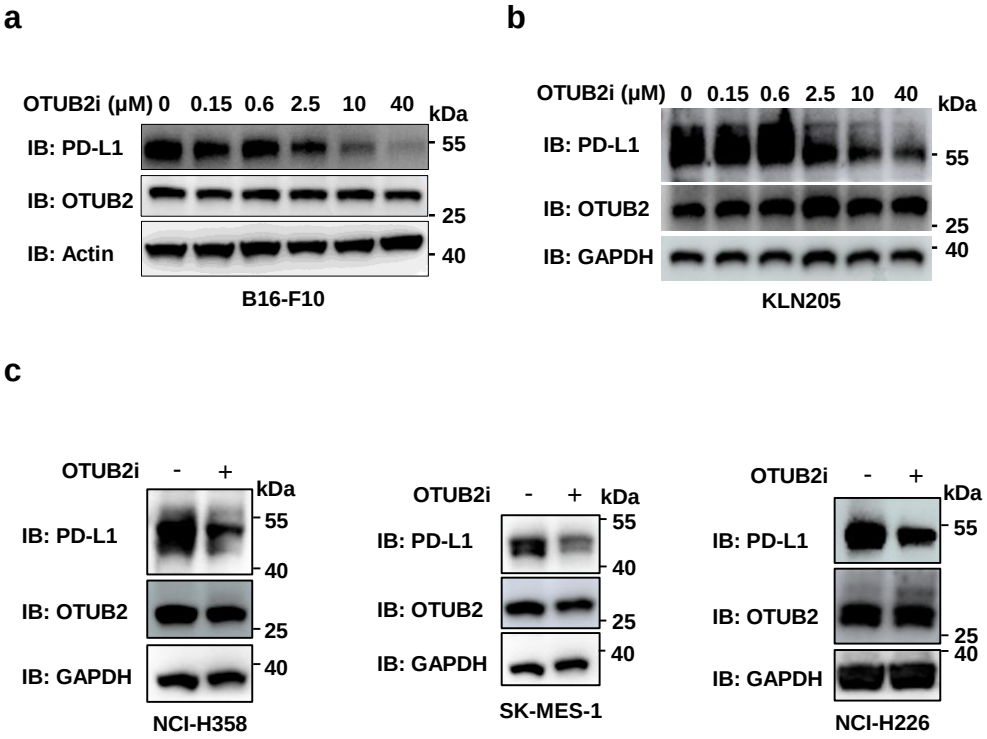

Supplementary Fig. 20. Effects of OTUB2-IN-1 on PD-L1 stability in different tumor cells. a, Inhibitory effects of OTUB2-IN-1 on the cellular level of PD-L1 in B16-F10 tumor cells. **b,** Inhibitory effects of OTUB2-IN-1 on the cellular level of PD-L1 in KLN205 tumor cells. **c,** Inhibitory effects of OTUB2-IN-1 (10 μM) on the cellular level of PD-L1 in multiple human lung cancer cell lines (NCI-H358, SK-MES-1 and NCI-H226). Source data are provided as a Source Data file.

Supplementary Fig. 21

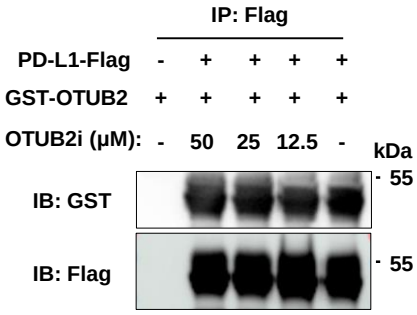

Supplementary Fig. 21. Determine the ability of OTUB2-IN-1 to block the binding of OTUB2 to PD-L1. The *in vitro* interaction between purified PD-L1-Flag proteins and GST-OTUB2 proteins in the presence of increasing concentration of the inhibitor examined by *in vitro* Flag pull-down assays. Source data are provided as a Source Data file.

Supplementary Fig. 22

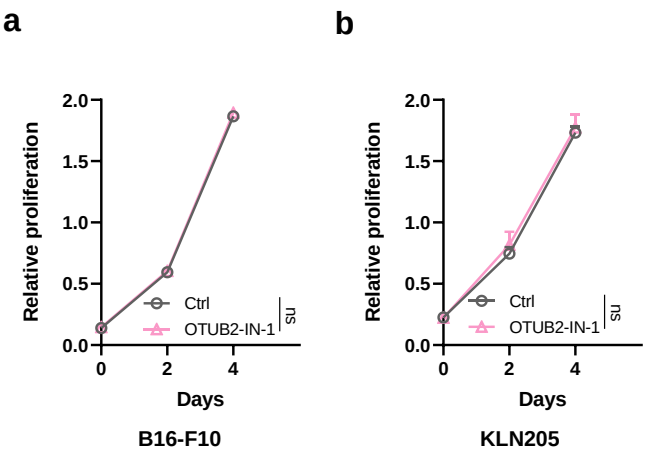

Supplementary Fig. 22. Effects of OTUB2-IN-1 on tumor cell growth *in vitro*. a, Effects of OTUB2-IN-1 (10 μM) on B16-F10 tumor cell growth. **b,** Effects of OTUB2-IN-1 (10 μM) on KLN205 tumor cell growth. n = 3 biologically independent experiments. The data are presented as the mean ± s.e.m., and P values were calculated using two-way analysis of variance (ANOVA). ns, not significant.

Supplementary Fig. 23

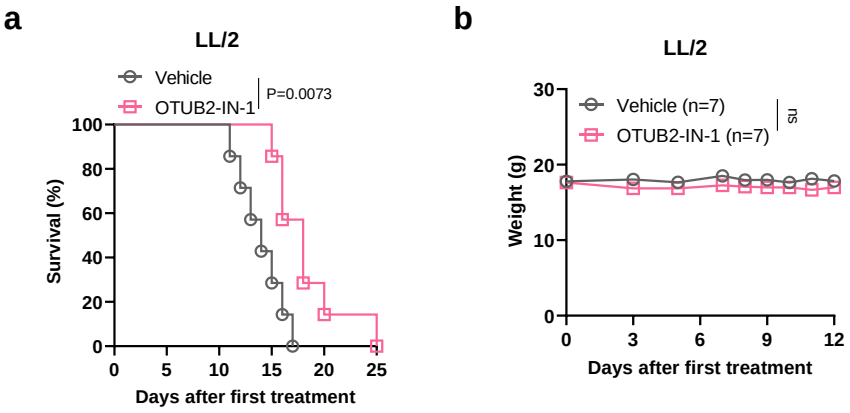

Supplementary Fig. 23. Effects of OTUB2-IN-1 on LL/2 tumor growth. a, Kaplan–Meier survival analysis of vehicle-or OTUB2-IN-1-treated host animals bearing LL/2 tumors. n = 7 mice per group. **b,** Weight monitoring of vehicle- or OTUB2-IN-1-treated host animals bearing LL/2 tumors. n = 7 mice per group. The data are presented as the mean ± s.e.m., and P values were calculated by the log-rank test (**a**), except for in **b,** in which P values were calculated using two-way analysis of variance (ANOVA). ns, not significant.

Supplementary Fig. 24

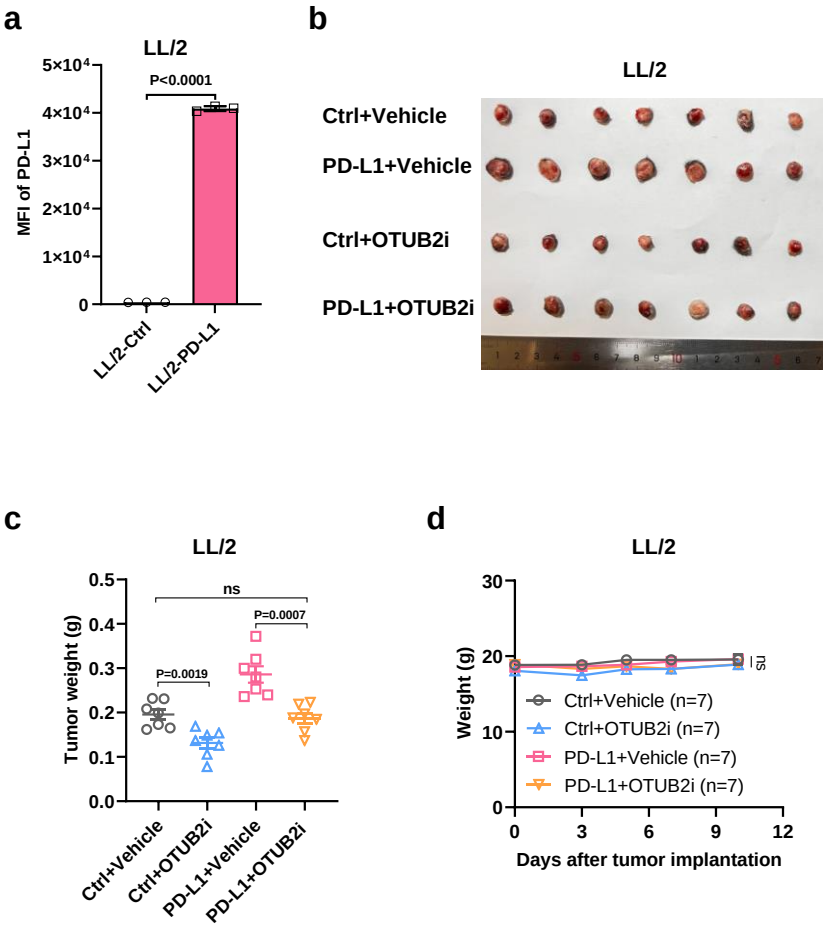

Supplementary Fig. 24. Effects of OTUB2-IN-1 on PD-L1-overexpressing tumor cell growth *in vivo*. a, Flow cytometry analysis of PD-L1 levels on the surface of control and PD-L1-overexpressing LL/2 tumor cells. n = 3 biologically independent experiments. **b,** Treatment with OTUB2-IN-1 reduced tumor growth in C57BL/6 mice implanted with control or PD-L1-overexpressing tumor cells. n = 7 mice per group. Photographs of tumors of each group at the end of the experiment. **c,** Tumor weight for each group at the end of the experiment. **d,** Weight monitoring of vehicle- or OTUB2-IN-1-treated host animals bearing control or PD-L1-overexpressing tumors. The data are presented as the mean ± s.e.m., and P values were calculated using an unpaired two-sided Student's t test (**a** and **c**), except for in **d,** in which P values were calculated using two-way analysis of variance (ANOVA). Source data are provided as a Source Data file. ns, not significant.

Supplementary Fig. 25

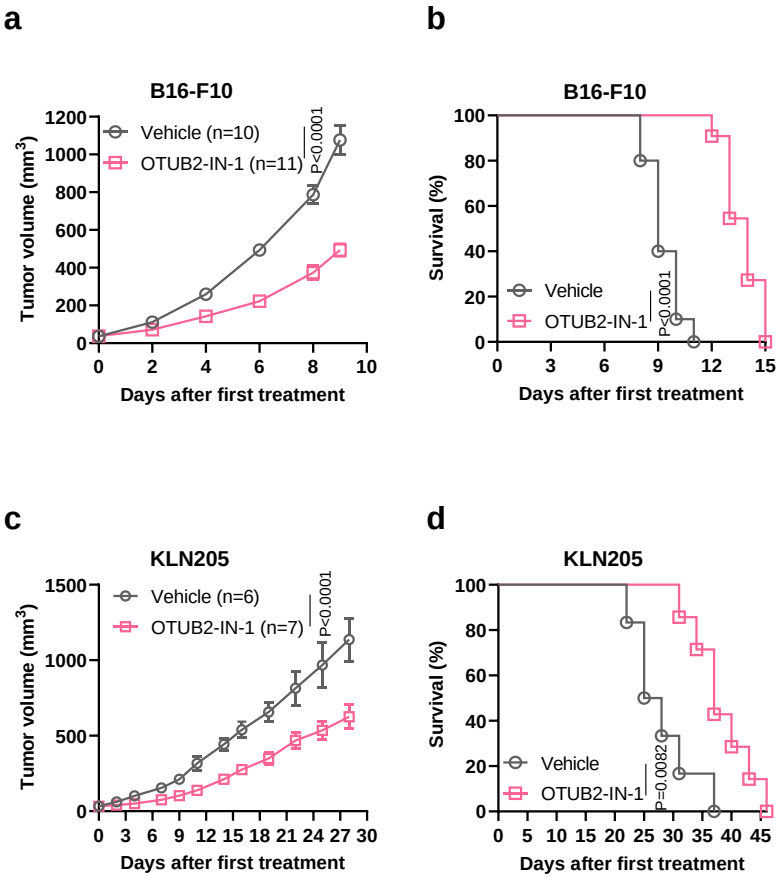

Supplementary Fig. 25. Effects of OTUB2-IN-1 on tumor cell growth *in vivo*. a, Treatment with OTUB2-IN-1 (20 mg/kg) reduced tumor growth in C57BL/6 mice implanted with B16-F10 tumor cells. n = 10 and 11 mice in the two groups. Mice were euthanized when the tumors reached 1000 mm^3 in volume or became necrotic. **b,** Kaplan–Meier survival analysis of vehicle- or OTUB2-IN-1-treated host animals bearing B16-F10 tumors. **c,** Treatment with OTUB2-IN-1 (20 mg/kg) reduced tumor growth in DBA/2 mice implanted with KLN205 tumor cells. n = 6 and 7 mice in the two groups. Mice were euthanized when the tumors reached 1000 mm^3 in volume or became necrotic. **d,** Kaplan–Meier survival analysis of vehicle- or OTUB2-IN-1-treated host animals bearing KLN205 tumors. The data are presented as the mean ± s.e.m., and P values were calculated using two-way analysis of variance (ANOVA) (**a** and **c**), except for in **b and d,** in which P values were calculated by the log-rank test.

Supplementary Fig. 26

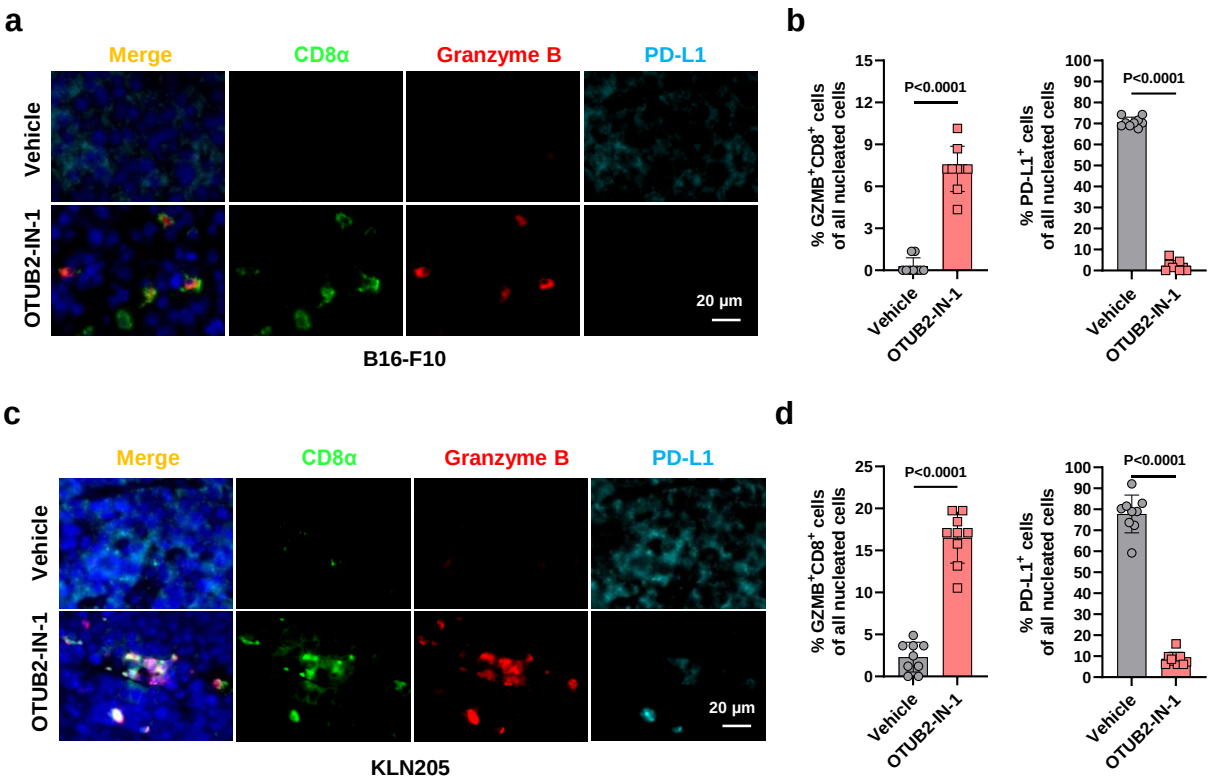

Supplementary Fig. 26. Effects of OTUB2-IN-1 on regulating PD-L1 abundance and intratumoral infiltration of $CD8^+$ and $GZMB^+$ CTLs in mouse tumors. a, Representative images of IHC staining with DAPI, anti-CD8α, anti-GZMB and anti-PD-L1 in B16-F10 tumors grown in syngeneic C57BL/6 mice after treatment with vehicle or OTUB2-IN-1. Scale bars, 20 μm. **b,** Quantitative estimates of $GZMB^+$ $CD8^+$ and $PD\text{-}L1^+$ cells in vehicle- or OTUB2-IN-1-treated tumors. Three fluorescent fields for each of the three samples were counted. n = 9 biologically independent samples. **c,** Representative images of IHC staining with DAPI, anti-CD8α, anti-GZMB and anti-PD-L1 in KLN205 tumors grown in syngeneic DBA/2 mice after treatment with vehicle or OTUB2-IN-1. Scale bars, 20 μm. **d,** Quantitative estimates of $GZMB^+$ $CD8^+$ and $PD\text{-}L1^+$ cells in vehicle- or OTUB2-IN-1-treated tumors. Three fluorescent fields for each of the three samples were counted. n = 9 biologically independent samples. The data are presented as the mean ± s.e.m., and P values were calculated by an unpaired two-sided Student's t test (**b** and **d**).

Supplementary Fig. 27

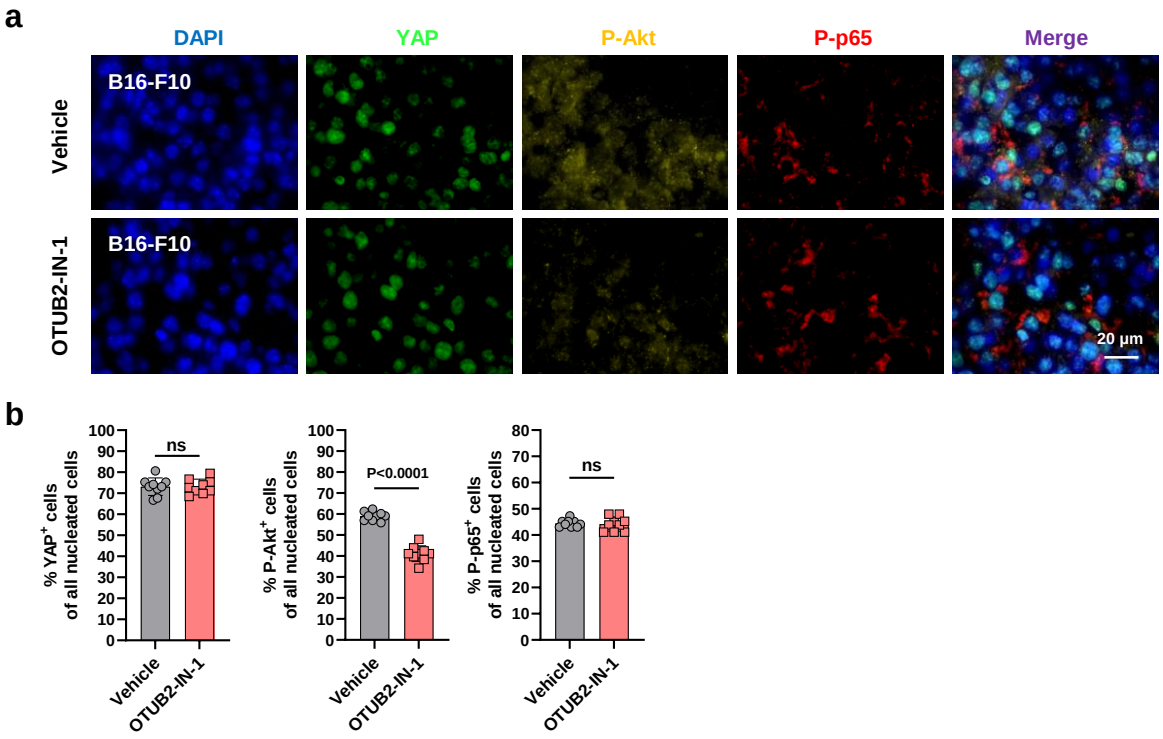

Supplementary Fig. 27. Effects of OTUB2-IN-1 on regulating Hippo, NF-κB and Akt/mTOR pathways in B16-F10 tumors. a, Representative images of IHC staining with DAPI, anti-YAP, anti-P-Akt and anti-P-p65 in B16-F10 tumors grown in syngeneic C57BL/6 mice after treatment with vehicle or OTUB2-IN-1. Scale bars, 20 μm. **b,** Quantitative estimates of YAP^+, $P\text{-}Akt^+$ and $P\text{-}p65^+$ cells in vehicle- or OTUB2-IN-1-treated tumors. Three fluorescent fields for each of the three samples were counted. n = 9 biologically independent samples. The data are presented as the mean ± s.e.m., and P values were calculated by an unpaired two-sided Student's t test (**b**). ns, not significant.

Supplementary Fig. 28

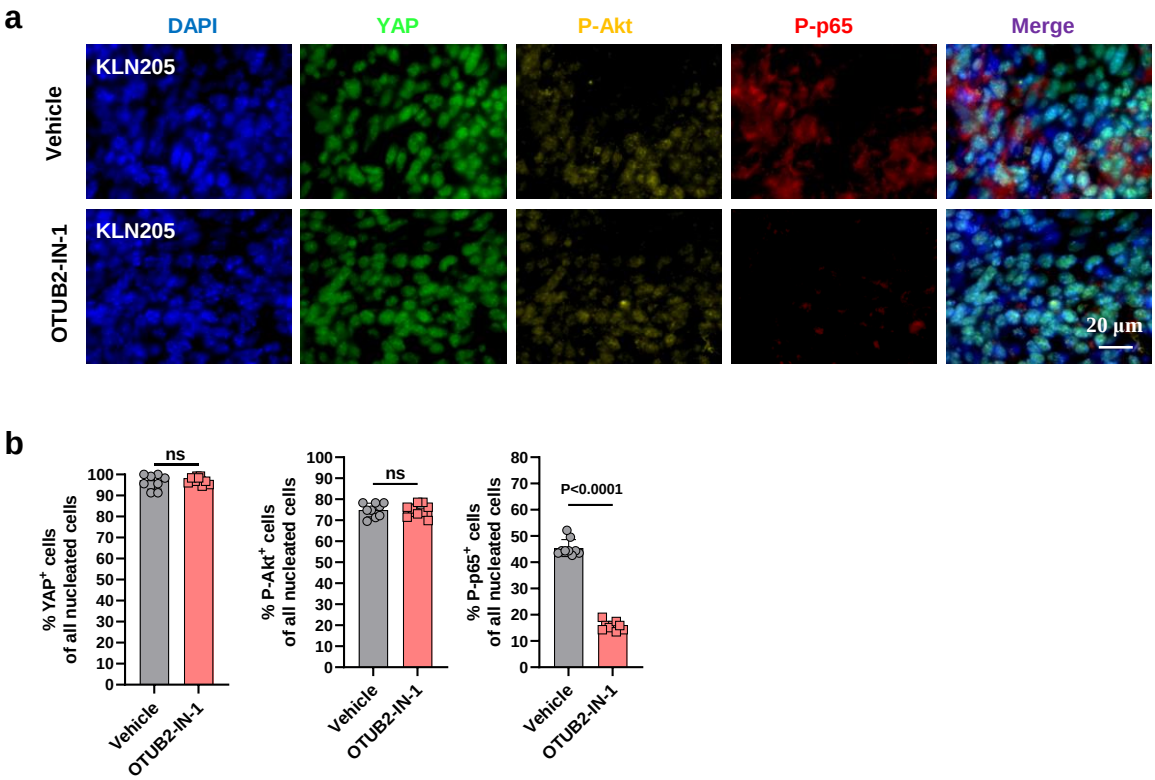

Supplementary Fig. 28. Effects of OTUB2-IN-1 on regulating Hippo, NF-κB and Akt/mTOR pathways in KLN205 tumors. a, Representative images of IHC staining with DAPI, anti-YAP, anti-P-Akt and anti-P-p65 in KLN205 tumors grown in syngeneic DBA/2 mice after treatment with vehicle or OTUB2-IN-1. Scale bars, 20 μm. **b,** Quantitative estimates of YAP^+, $P\text{-}Akt^+$ and $P\text{-}p65^+$ cells in vehicle- or OTUB2-IN-1-treated tumors. Three fluorescent fields for each of the three samples were counted. n = 9 biologically independent samples. The data are presented as the mean ± s.e.m., and P values were calculated by an unpaired two-sided Student's t test (**b**). ns, not significant.

Supplementary Fig. 29

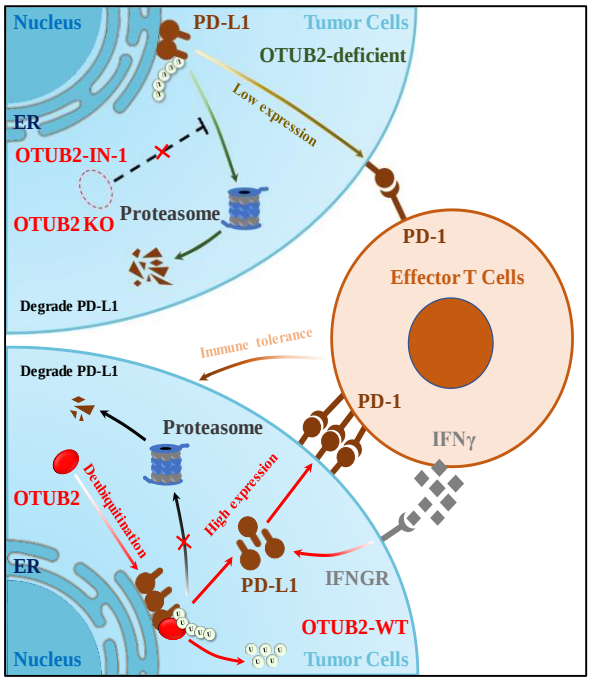

Supplementary Fig. 29. Diagram illustrating OTUB2-mediated deubiquitination of PD-L1 in the ER. Top, in the absence of OTUB2 (through genetic deletion or OUTB2 inhibitors), PD-L1 is transported into ERs and degraded. Down, in the presence of OTUB2, PD-L1 levels on the surface remain high and can thus reduce tumor cell sensitivity to $CD8^+$ T-cell-mediated cytotoxicity.

Supplementary Table 1. DUBs gene list used in this study.

Ubiquitin-specific proteases (USPs)	Cysteine proteases ubiquitin C-terminal hydrolases (UCHs)	Ovarian tumor proteases (OTUs)	Machado-Joseph domain proteases (MJDs)	Metalloproteases JAB1/MPN/MOV34 (JAMM)	MCPIP family	Novel
USP1	UCHL1	ALG13	ATXN3	BRCC3	KHNYN	PPPDE1
USP2	UCHL3	OTUB1	JOSD1	COPS5	N4BP1	HAUSP
USP3	UCHL5	OTUB2	JOSD2	COPS6/CSN6	NYNRIN	
USP4	BAP1	OTUD1	ATXN3L	EIF3F	ZC3H12A	
USP5		OTUD3		EIF3H	ZC3H12B	
USP6		OTUD4		MPND	ZC3H12C	
USP6NL		OTUD5		MYSM1	ZC3H12D	
USP7		OTUD6A		PRPF8		
USP8		OTUD6B		PSMD14		
USP9X		OTUD7A		PSMD7		
USP9Y		OTUD7B		STAMBP		
USP10		OTULIN		STAMBPL1		
USP11		VCPIP1				
USP12		ZRANB1				
USP13		YOD1				
USP14		TNFAIP3				
USP15						
USP16						
USP17						
USP17L2						
USP17L6P						
USP18						
USP19						
USP20						
USP21						
USP22						
USP24						
USP25						
USP26						
USP27X						
USP28						
USP29						
USP30						
USP31						
USP32						
USP33						
USP34						
USP35						
USP36						
USP37						
USP38						
USP39						
USP40						
USP42						
USP43						
USP44						
USP45						
USP46						
USP47						
USP48						
USP49						
USP50						
USP51						
USP52						
USP53						
USP54						
CYLD						
USPL1						

Supplementary Table 2. The docking scores of the compounds capable of binding to the catalytic pocket of OTUB2.

Item	Drug_Names	docking score	MW
1	(5-(2-amino-5-isobutylthiazol-4-yl)furan-2-yl)phosphonic acid	-6.945	302.29
2	(E)-4-(4-(2-carboxyvinyl)phenylsulfonamido)butanoic acid	-6.811	313.33
3	2-((2-(3,4-dihydroxyphenyl)-2-oxoethyl)thio)nicotinic acid	-6.059	305.31
4	(E)-2-(5-(2-carboxyvinyl)-2-methylphenylsulfonamido)benzoic acid	-5.864	361.37
5	3-(2-hydroxy-6-methoxyquinolin-3-yl)propanoic acid	-5.812	247.25
6	2,2'-((9H-fluorene-2,7-disulfonyl)bis(azanediyl))diacetic acid	-5.783	440.45
7	(R)-2-(isobutylamino)-4-oxo-4-((4-sulfamoylphenyl)amino)butanoic acid	-5.691	343.40
8	(2R,3R)-3-(1H-benzo[d]imidazol-2-yl)-2,3-dihydroxypropanoic acid	-5.656	222.20
9	(R)-4-((3-(3-allylthioureido)phenyl)amino)-2-(butylamino)-4-oxobutanoic acid	-5.649	378.49
10	(R)-4-((3-(3-allylthioureido)phenyl)amino)-2-(isobutylamino)-4-oxobutanoic acid	-5.613	378.49
11	(R)-3-((3-(carboxymethyl)-2,4-dioxothiazolidin-5-yl)amino)benzoic acid	-5.582	310.28
12	2-(5-oxo-2,5-dihydro-1H-pyrazol-3-yl)acetic acid	-5.503	142.11
13	3-(4-amino-3-((2-((4-nitrophenyl)amino)-2-oxoethyl)thio)-5-oxo-4,5-dihydro-1,2,4-triazin-6-yl)propanoic acid	-5.363	394.36
14	(E)-6-(5-(1-(carboxymethyl)-2-oxoindolin-3-ylidene)-4-oxo-2-thioxothiazolidin-3-yl)hexanoic acid	-5.345	434.49
15	2-(2-(3,5-dimethoxybenzamido)thiazol-4-yl)acetic acid	-5.286	322.34
16	(R)-4-((3-(3-allylthioureido)phenyl)amino)-4-oxo-2-(pentylamino)butanoic acid	-5.281	392.52
17	(R)-2-hydroxy-2-(pyridin-2-yl)propanoic acid	-5.279	167.16
18	(Z)-2-(5-(4-hydroxy-3-methoxy-5-nitrobenzylidene)-4-oxo-2-thioxothiazolidin-3-yl)acetic acid	-5.259	370.36
19	(R)-4-((3-(3-allylthioureido)phenyl)amino)-2-((furan-2-ylmethyl)amino)-4-oxobutanoic acid	-5.242	402.47
20	2-(2-((pyridin-4-ylmethyl)thio)thiazol-4-yl)acetic acid	-5.242	266.34

Supplementary Table 3. shRNA sequences.

Gene	Sequence (5'-3')
shControl	CCTAAGGTTAAGTCGCCCTCG
sh-mOTUB2 #1	GATGAGGAGATGGACATCAAA
sh-mOTUB2 #2	CTTCGGTTTATCTGCTCTATA
sh-mOTUB2 #3	GAAGACCAAAGGAGACGGAAA
sh-mOTUB2 #4	CTATCCATTCTTCGGGAT CAT
sh-hOTUB2 #1	CCTATGTGTCACTGGATTATT
sh-hOTUB2 #2	TGTGGTGGAACTGGTAGAGAA
sh-hOTUB2 #3	CGAGATGGATACCGCCCTGAA
sh-hOTUB2 #4	CATCCCACTACAACATCCTTT
sh-hOTUB2 #5	TGTGGTGGAACTGGTAGAGAA
sh-hOTUB1	AGCGACTCCGAAGGTGTTAAC
sh-hUSP22	TGTGCCAGGACTACATCTATG
sh-hCSN5	GAGCTGTTGTGGAATAAAT
sh-hUSP7	CTCAGAACCCTGTGATCAA
sh-hUSP9X	CGCCTGATTCTTCCAATGAAA

Supplementary Table 4. sgRNA sequences.

Gene	Sequence (5'-3')
sgControl	GAACGACTAGTTAGGCGTGTA
sg-mOTUB2 #1	GCAAAAGATTCACCTCGATC
sg-mOTUB2 #1	GGTAGAGTACGTCGACGAGA
sg-hOTUB2 #1	TTCAACGACCAGAGTGCCT

Supplementary Table 5. Plasmids.

Plasmid	Source	Catalog No.
pLKO.1	Addgene	10878
psPAX2	Addgene	12260
PMD2.G	Addgene	12259
pCI-neo-cOVA	Addgene	25097
lentiCRISPR v2	Addgene	52961
lentiCas9-Blast	Addgene	52962

Supplementary Table 6. Antibodies.

Antibody	Source	Catalog No.	Application (Dilution)
APC anti-mouse CD274 antibody	Biolegend	124312	FCM(1:200)
APC anti-human CD274 antibody	Biolegend	329708	FCM(1:200)
BV605 anti-mouse CD45 antibody	Biolegend	103140	FCM(1:200)
FITC mouse CD8a antibody	Biolegend	100706	FCM(1:200)
APC anti-mouse IFN-γ antibody	Biolegend	505810	FCM(1:200)
PE/Cyanine7 anti-human/mouse granzyme B recombinant antibody	Biolegend	372214	FCM(1:200)
Zombie Aqua Fixable Viability Kit	Biolegend	423102	FCM(1:200)
Anti-OTUB2 mouse monoclonal antibody	Sangon Biotech	D199590-0100	WB(1:500) IP(1:100)
Anti-PD-L1-mouse	Abcam	ab213480	WB(1:500) IP(1:100)
PD-L1 monoclonal antibody	Proteintech	66248-1-Ig	WB(1:500)
Monoclonal anti-HA antibody	SIGMA-ALDRICH	H3663-200UL	WB(1:2,000)
Monoclonal anti-FLAG® M2 antibody	SIGMA-ALDRICH	F1804-200UG	WB(1:2000)
Anti-c-Myc antibody	SIGMA-ALDRICH	C3956	WB(1:500)
Ubiquitin (P4D1) mouse mAb	CST	3936	WB(1:1,000)
beta actin antibody	Proteintech	66009-1-Ig	WB(1:2,000)
GAPDH antibody	Proteintech	60004-1-Ig	WB(1:2,000)
Goat Anti-Rabbit IgG (H + L)-HRP Conjugate	Bio-Rad	1706515	WB(1:3,000)
Goat Anti-Mouse IgG (H + L)-HRP Conjugate	Bio-Rad	1706516	WB(1:3,000)
anti-GST-HRP	Proteintech	HRP-66001	WB(1:500)
anti-GST antibody	Sino Biological	11213-RP01	ELISA(1:2,000)
OTUB2 antibody	Affinity	AF9147	IHC(1:3,000)
Calnexin (C5C9) rabbit mAb	CST	2679S	IF(1:1,000)
Alexa Fluor® 488 donkey anti-mouse IgG (H+L)	Invitrogen	A-21202	IF(1:2,000)
TRITC-conjugated goat anti-rabbit IgG	SIGMA-ALDRICH	T6778-1ML	IF(1:500)
Alexa Fluor 488-conjugated donkey anti-rabbit IgG	Invitrogen	A-21206	IF(1:2000)
Alexa Fluor 647-conjugated goat anti-mouse IgG	Invitrogen	A-21237	IF(1:500)
CD8α (D4W2Z) XP® rabbit mAb	CST	98941	IHC(1:200)

Anti-granzyme B antibody	Abcam	ab4059	IHC(1:100)
Recombinant anti-CD8α antibody	Abcam	ab209775	IHC(1:1000)
PD-L1 Polyclonal antibody	Proteintech	17952-1-AP	IHC(1:1000)
OTUB1	Abcam	ab175200	WB(1:200)
CSN5	CST	6895S	WB(1:200)
USP9X	Proteintech	55054-1-AP	WB(1:2000)
USP7	CST	4833T	WB(1:2000)
USP22	Abcam	ab195289	WB(1:200)
YAP	Affinity	DF3182	IHC(1:100)
Phospho-AKT1 (S473)	Abcam	ab81283	IHC(1:100)
Phospho-p65 (S536)	Affinity	AF2006	IHC(1:100)
InVivoMAb anti-mouse CD8α	Bio X Cell	BE0061	200 μg/mouse
InVivoMAb rat IgG2b LTF-2	Bio X Cell	BE0090	200 μg/mouse

Supplementary Table 7. Reagents and chemical compounds.

Reagents	Source	Catalog No.
Recombinant Murine IFN-γ	BEYOTIME	P6137-100μg
Recombinant Human IFN-gamma Protein	R&D Systems	285-IF-100
Fixation/Permeabilization Solution Kit	BD	554714
Pierce™ IP Lysis Buffer	Thermo Scientific	87787
Dynabeads® Protein A	Invitrogen	100-02D
ANTI-FLAG® M2 Affinity Gel	SIGMA-ALDRICH	A2220
Pierce anti-HA Magnetic Beads	Thermo Scientific	88836
Lumi-Light^{PLUS} Western Blotting Substrate	Roche	12015196001
Glutathione sepharose 4B	GE	17075601
Protease Inhibitor Cocktail	MCE	HY-K0011
DAPI	Invitrogen	D1306
Cycloheximide	MCE	HY-12320
MG-132	MCE	HY-13259
Chloroquine diphosphate	MCE	HY-17589
Eeyarestatin I	MCE	HY-110078
SIINFEKL peptide	Sangon Biotech	
mouse recombinant IL-2	Sino Biological	51061-MNAE-20
Dynabeads™ Human T-Activator CD3/CD28	GIBCO	11131D
Human Recombinant IL-2	stemcell	78036
ER-Tracker™ Red	Thermo Fisher	E34250
Lyso-Tracker Red	BEYOTIME	C1046
OTUB2-IN-1	Life Chemicals	F0444-0064
OPAL 6-PLEX manual detection kit	AKOYA	NEL811001KT
Rhodamine 110-Ub	R&D Systems	U-550-050
1,10-phenanthroline	MCE	HY-W004544
N-Ethylmaleimide	Topscience	T3088
PR-619	MCE	HY-13814
TUBE2 magnetic beads	LifeSensors	UM-0402M-1000

Uncropped blots for Supplementary Fig. 6a

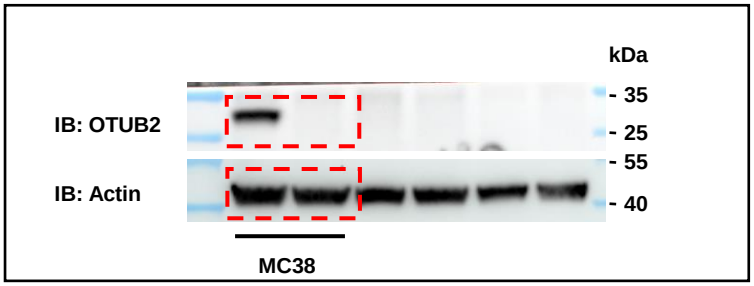

Uncropped blots for Supplementary Fig. 6b

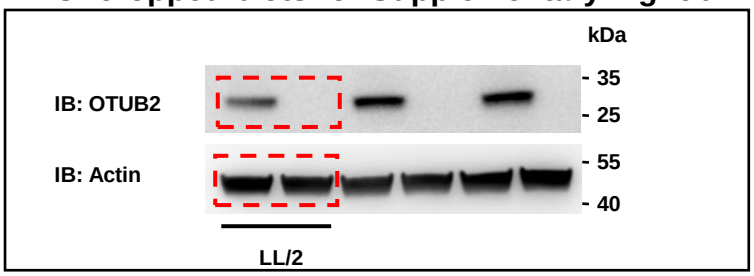

Uncropped blots for Supplementary Fig. 6c

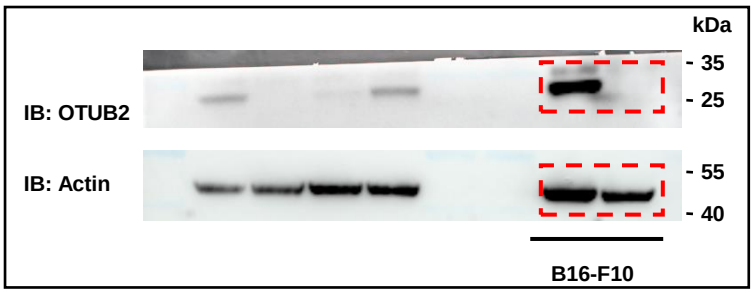

Uncropped blots for Supplementary Fig. 6g

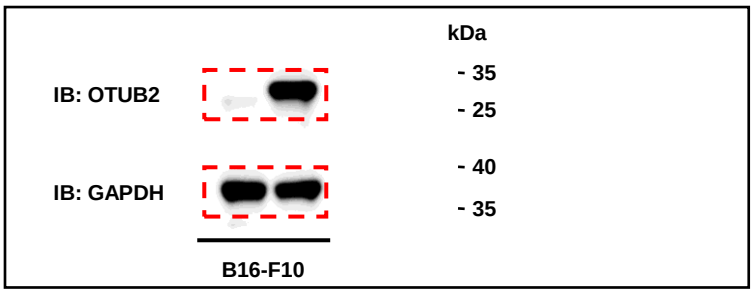

Uncropped blots for Supplementary Fig. 7a

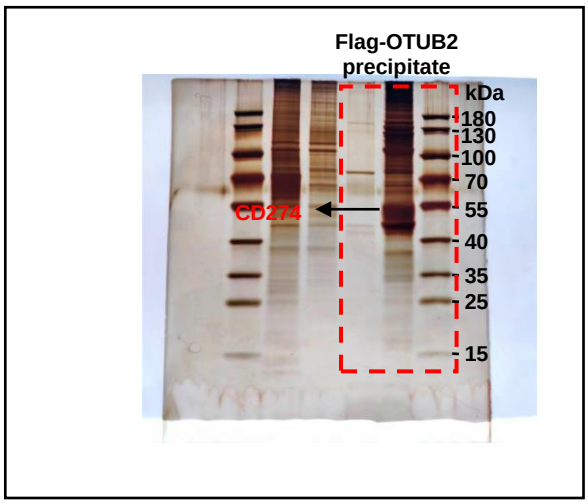

Uncropped blots for Supplementary Fig. 7b

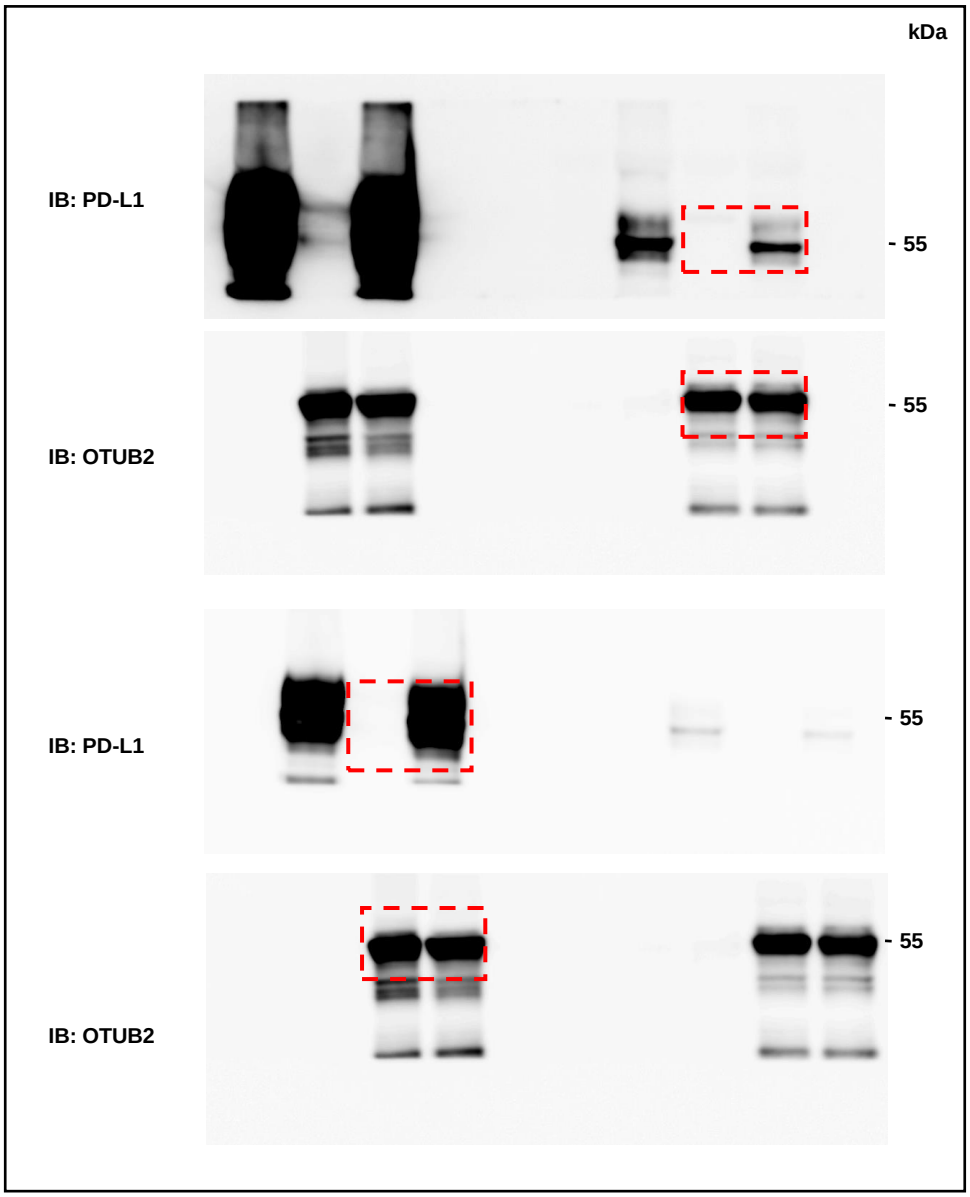

Uncropped blots for Supplementary Fig. 7c

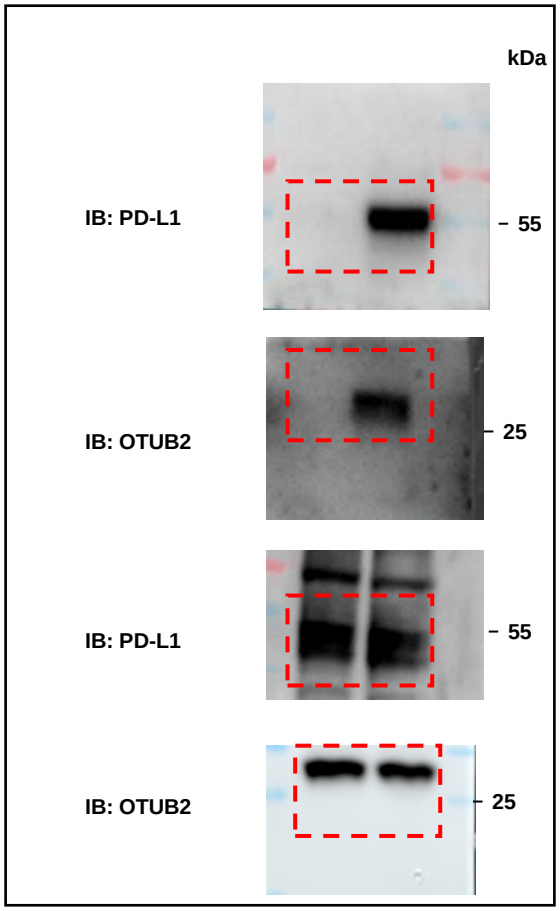

Uncropped blots for Supplementary Fig. 7d

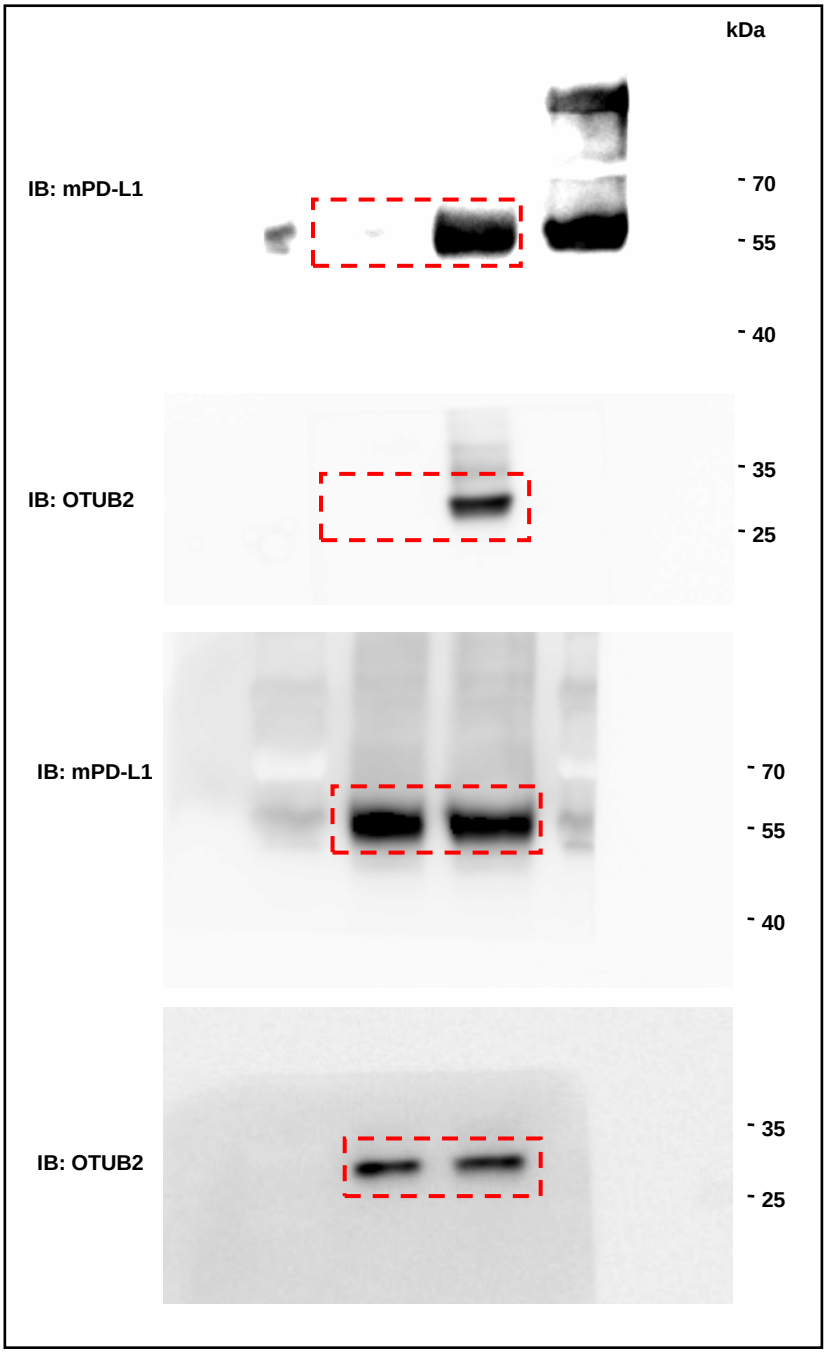

Uncropped blots for Supplementary Fig. 7e

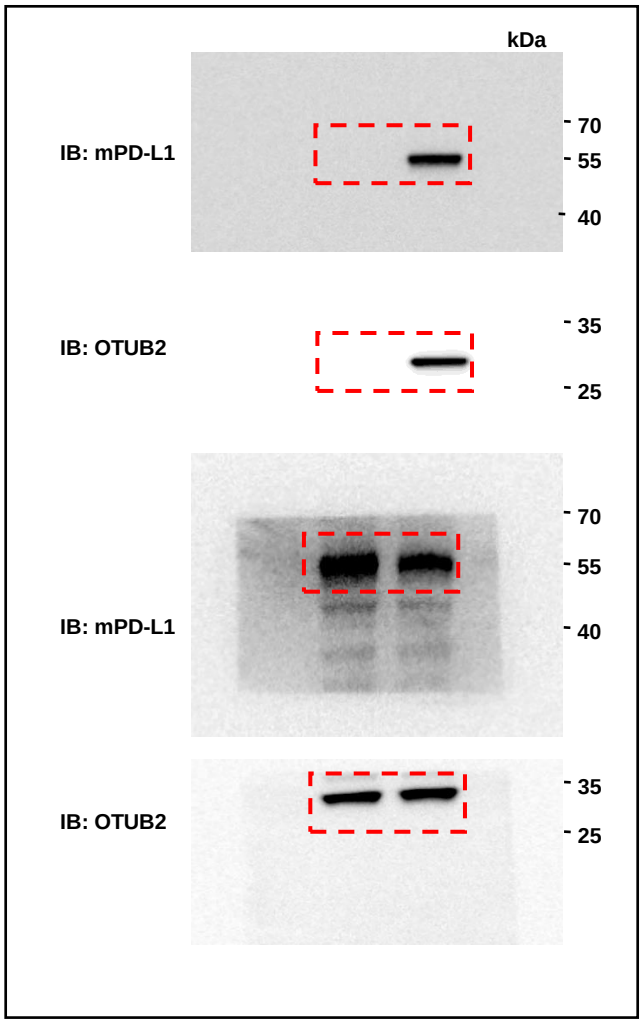

Uncropped blots for Supplementary Fig. 8a

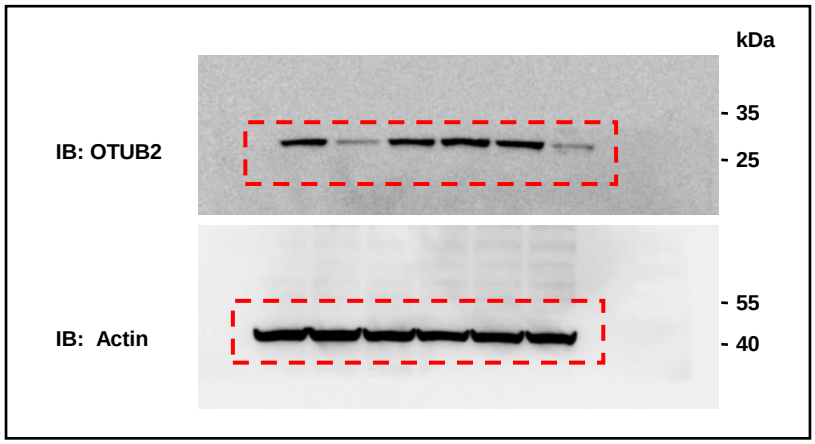

Uncropped blots for Supplementary Fig. 8e

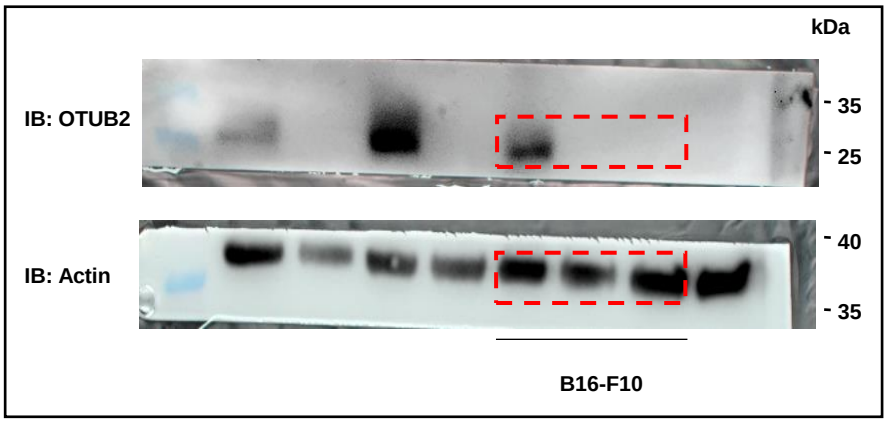

Uncropped blots for Supplementary Fig. 8g

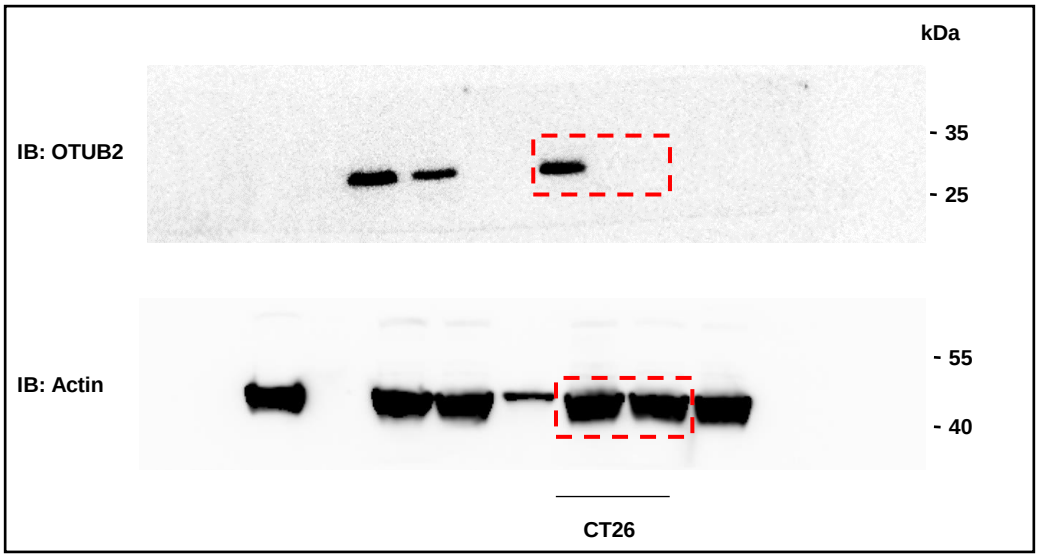

Uncropped blots for Supplementary Fig. 9a

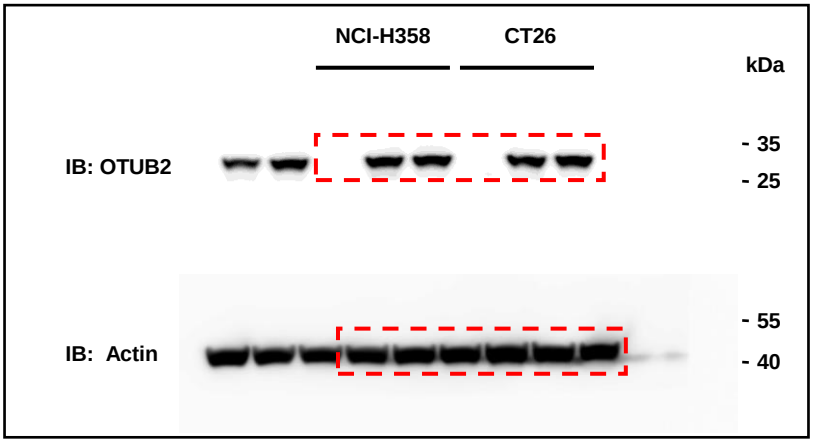

Uncropped blots for Supplementary Fig. 10a

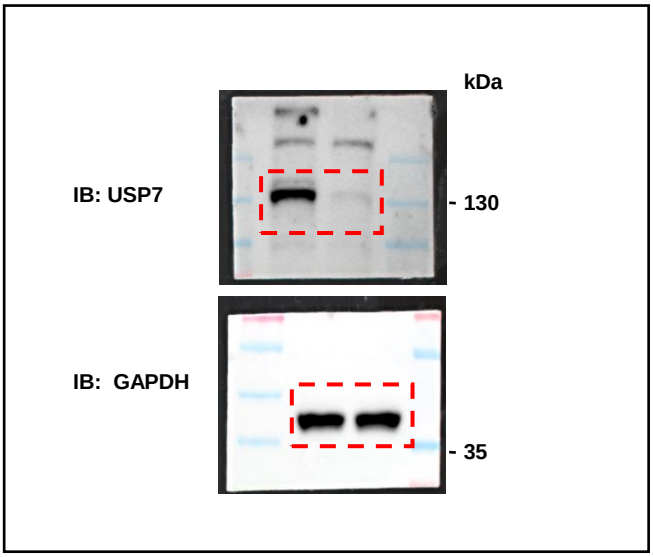

Uncropped blots for Supplementary Fig. 10b

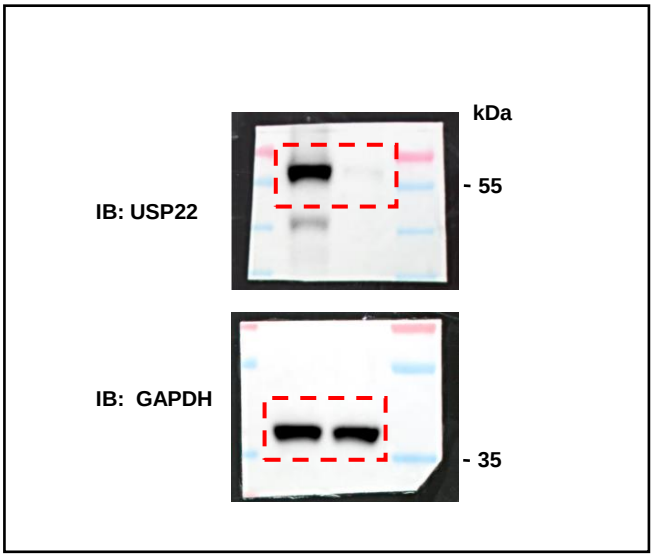

Uncropped blots for Supplementary Fig. 10c

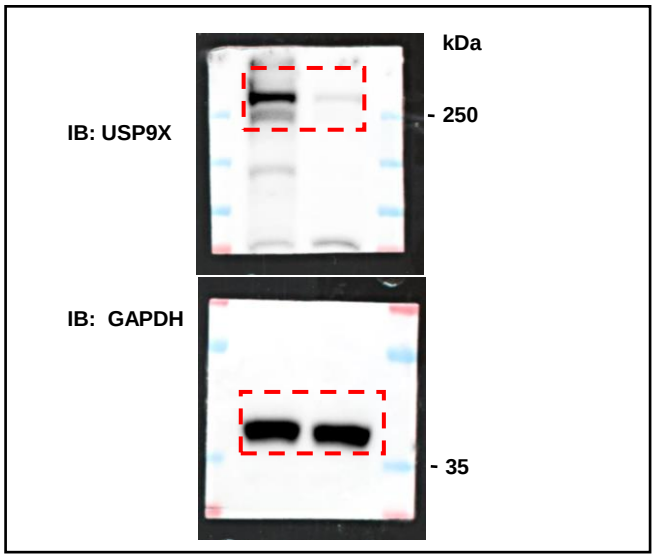

Uncropped blots for Supplementary Fig. 10d

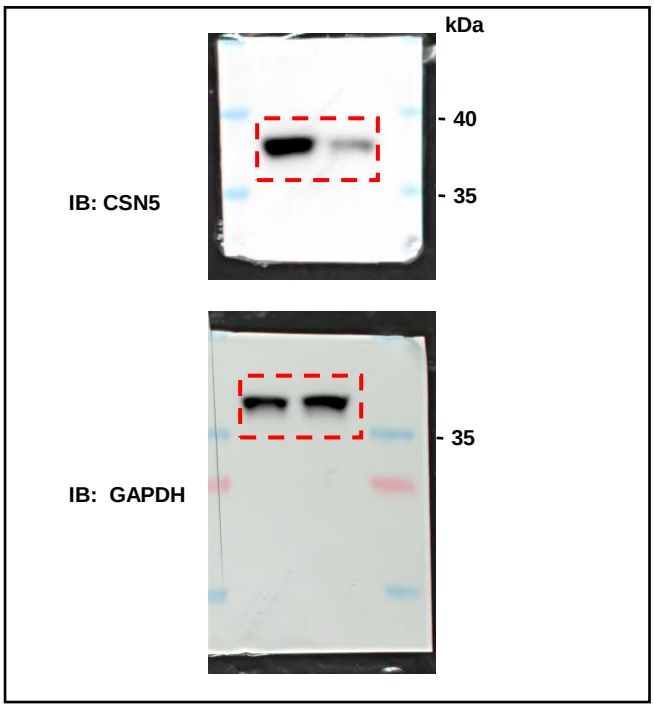

Uncropped blots for Supplementary Fig. 10e

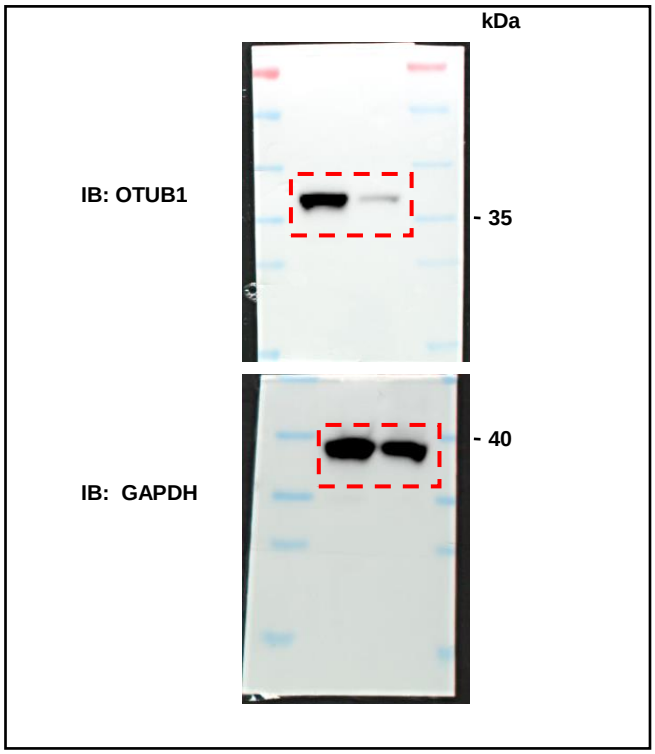

Uncropped blots for Supplementary Fig. 10f

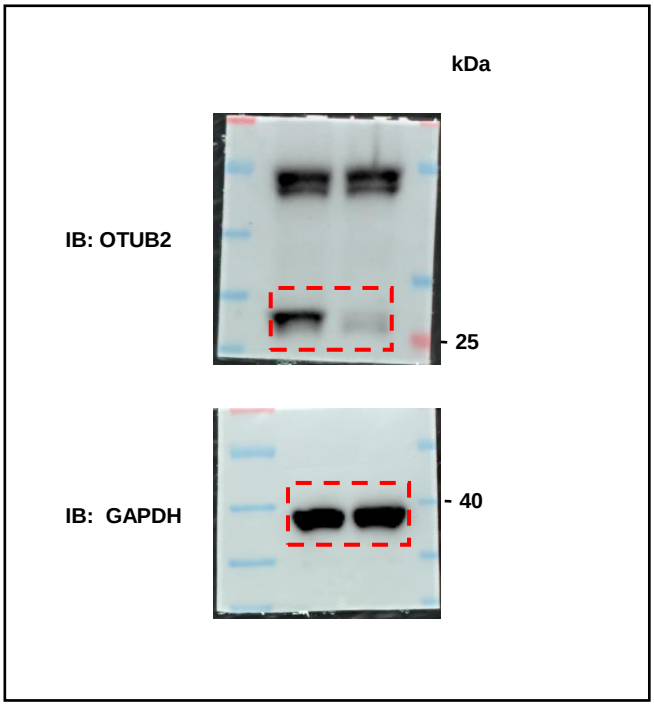

Uncropped blots for Supplementary Fig. 11a

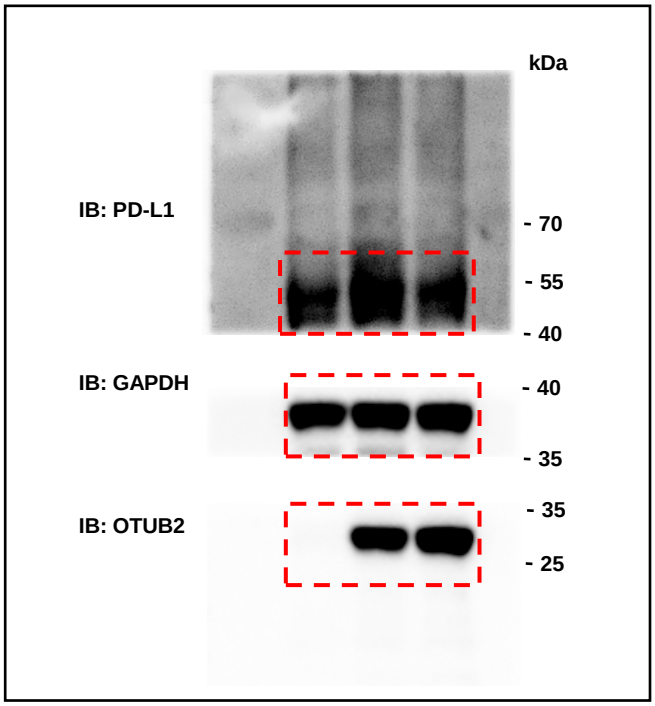

Uncropped blots for Supplementary Fig. 11b

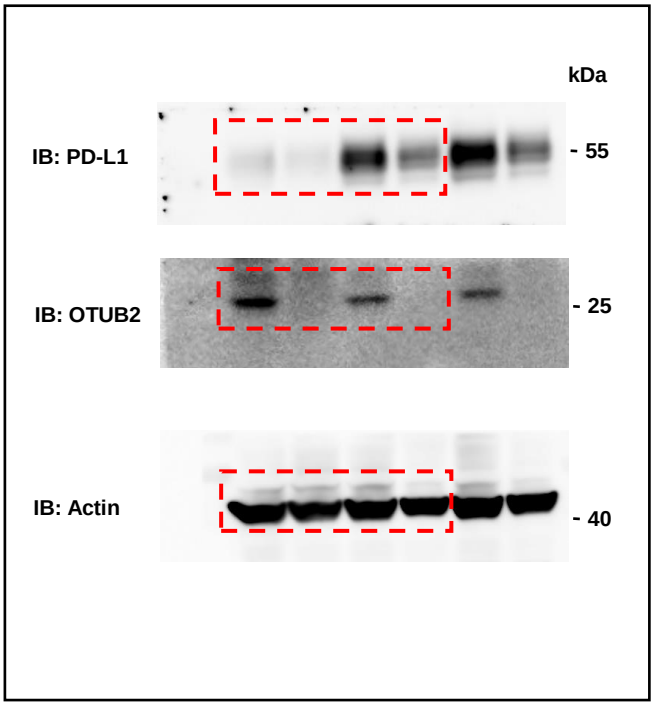

Uncropped blots for Supplementary Fig. 11c

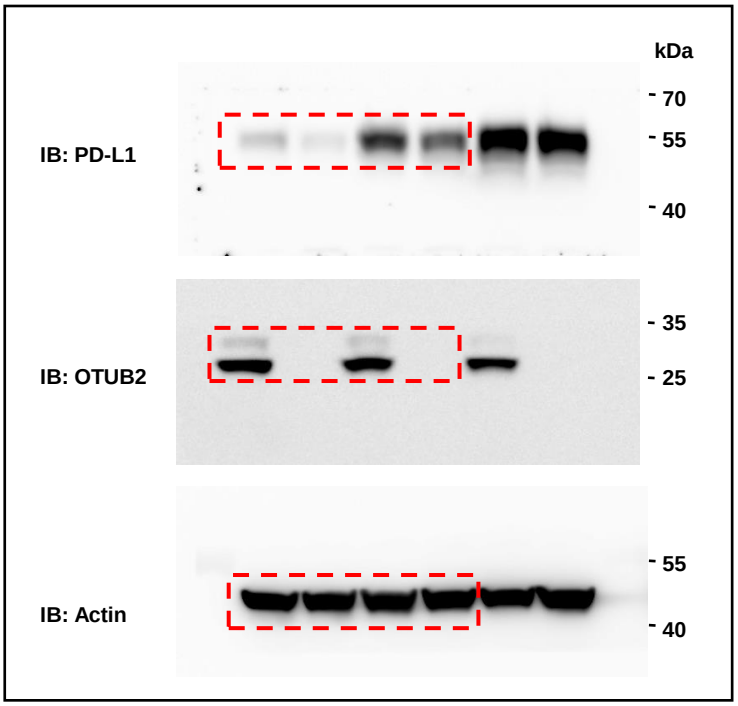

Uncropped blots for Supplementary Fig. 11d

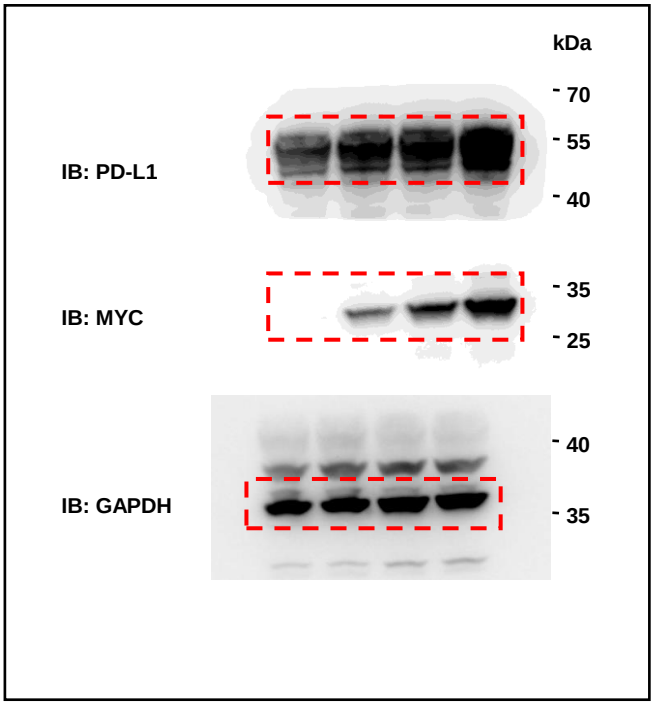

Uncropped blots for Supplementary Fig. 11e

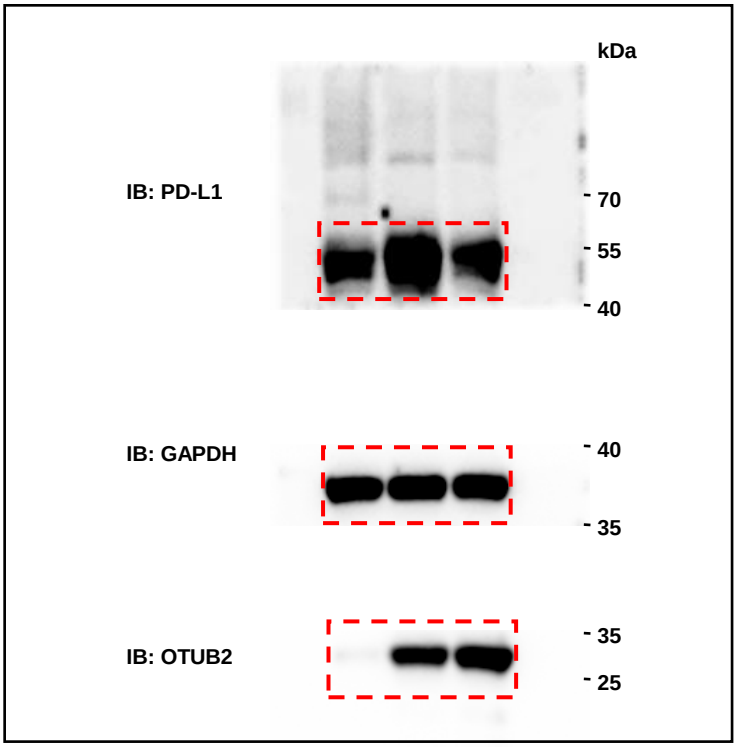

Uncropped blots for Supplementary Fig. 11f

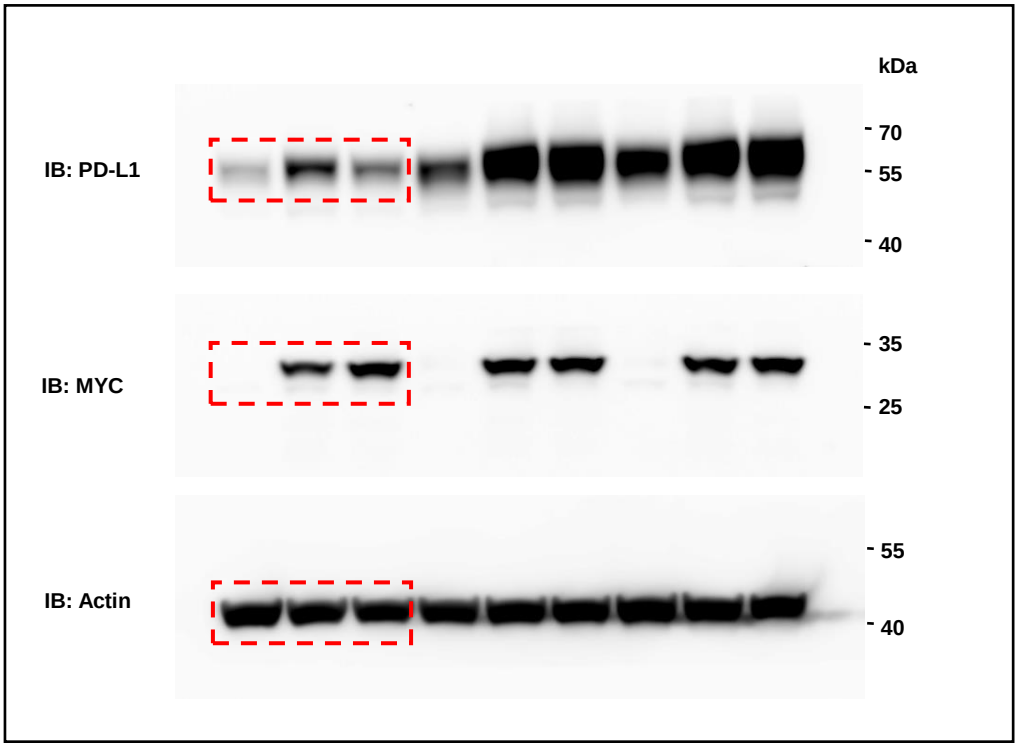

Uncropped blots for Supplementary Fig. 12a

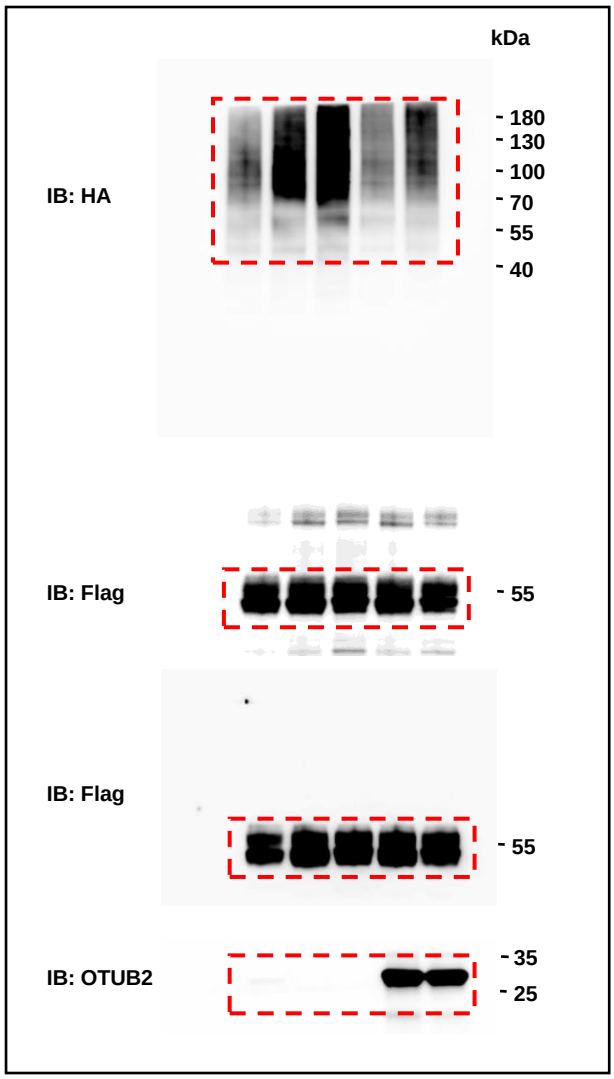

Uncropped blots for Supplementary Fig. 12b

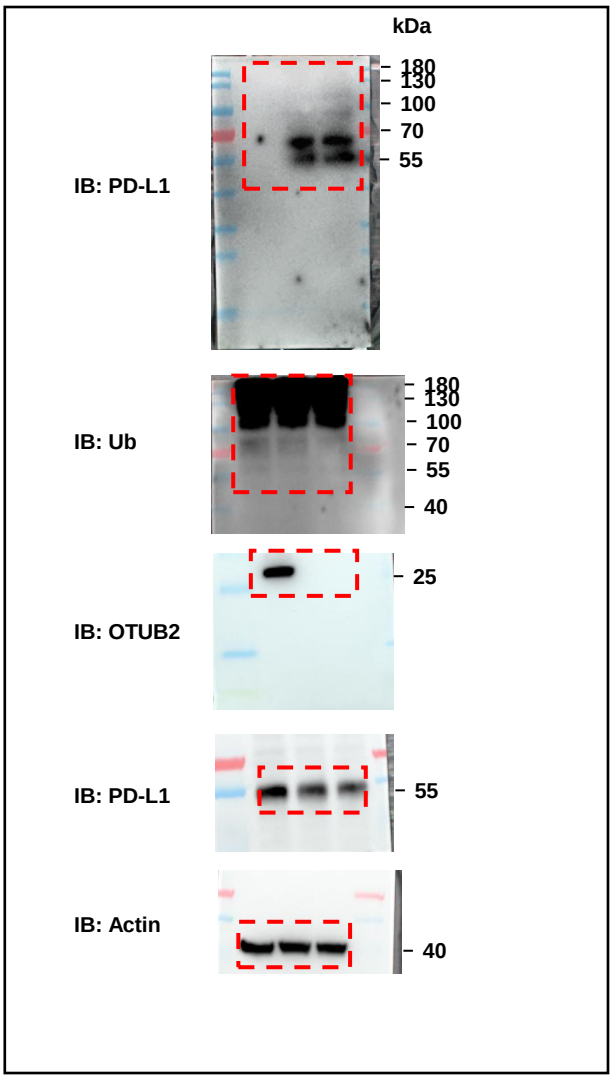

Uncropped blots for Supplementary Fig. 13a

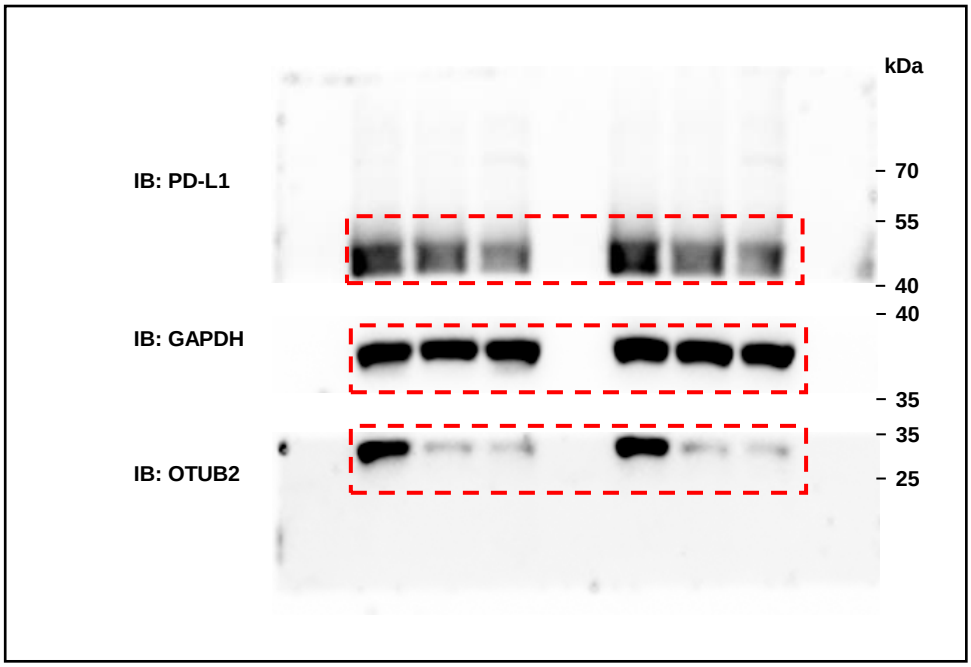

Uncropped blots for Supplementary Fig. 13b

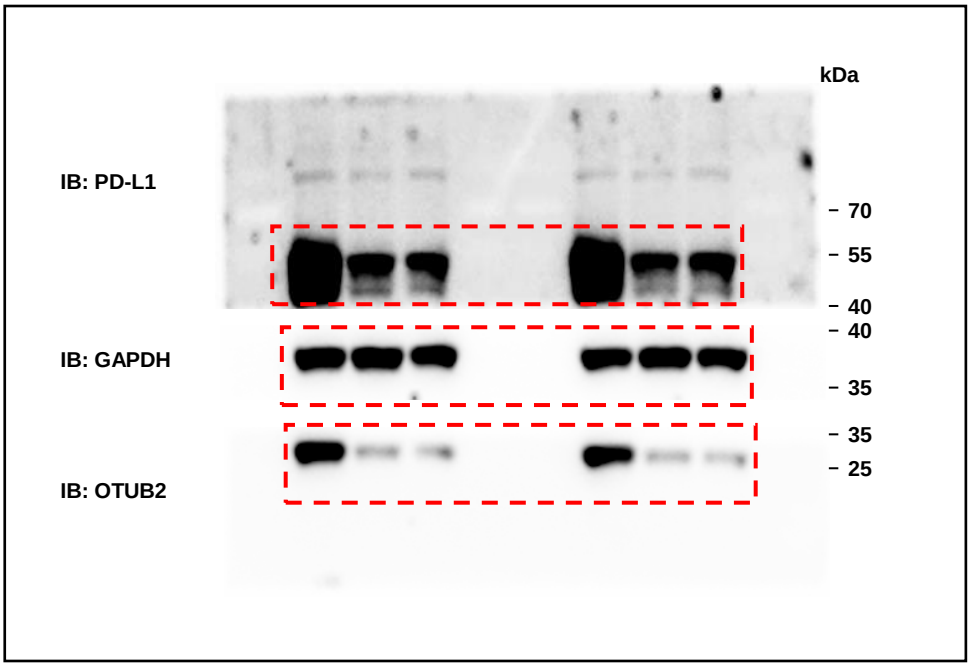

Uncropped blots for Supplementary Fig. 15a

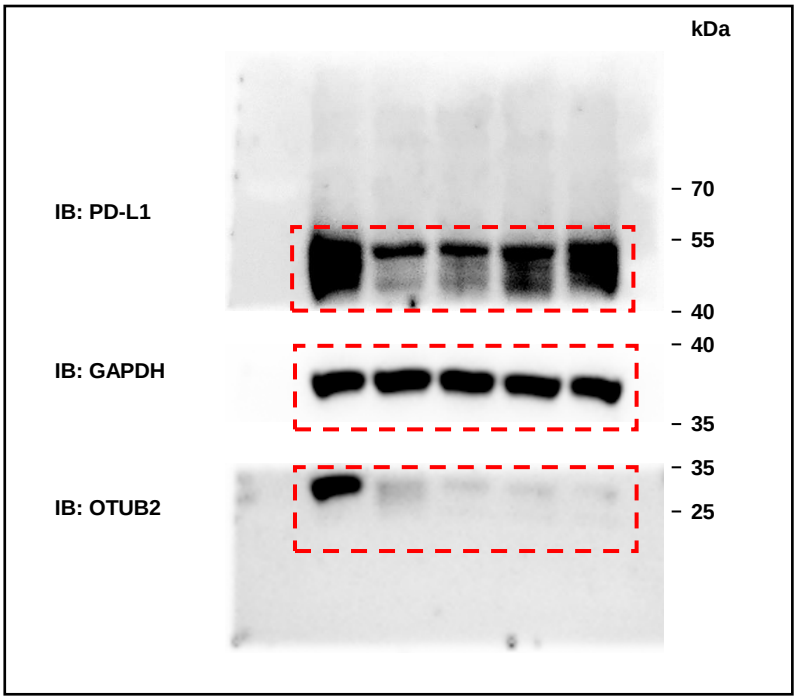

Uncropped blots for Supplementary Fig. 15b

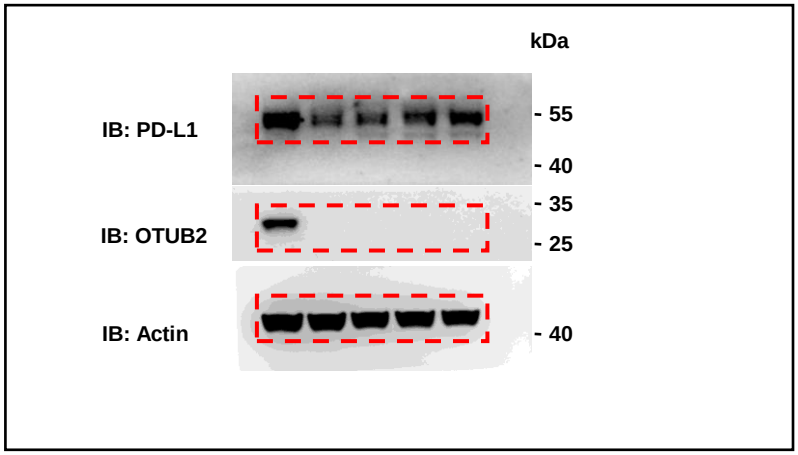

Uncropped blots for Supplementary Fig. 15c

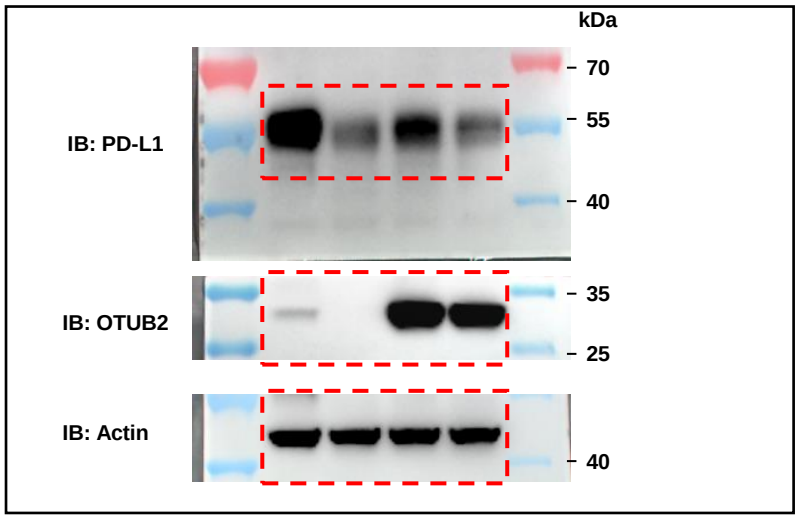

Uncropped blots for Supplementary Fig. 19b

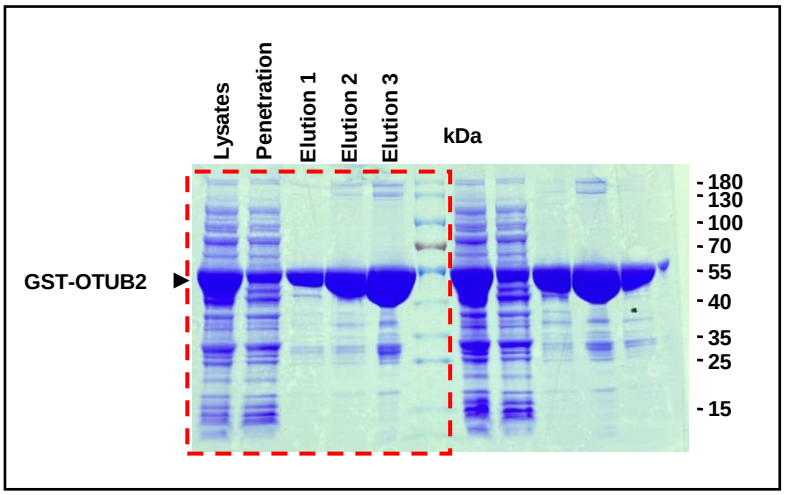

Uncropped blots for Supplementary Fig. 19e

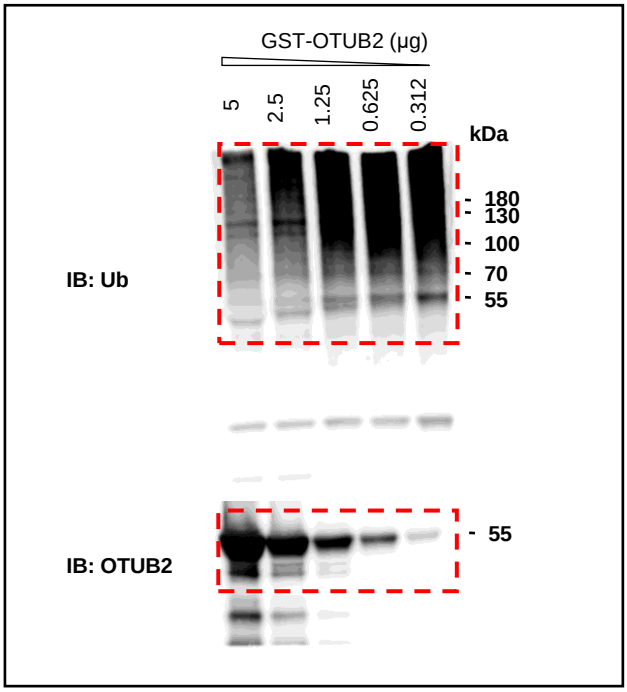

Uncropped blots for Supplementary Fig. 20a

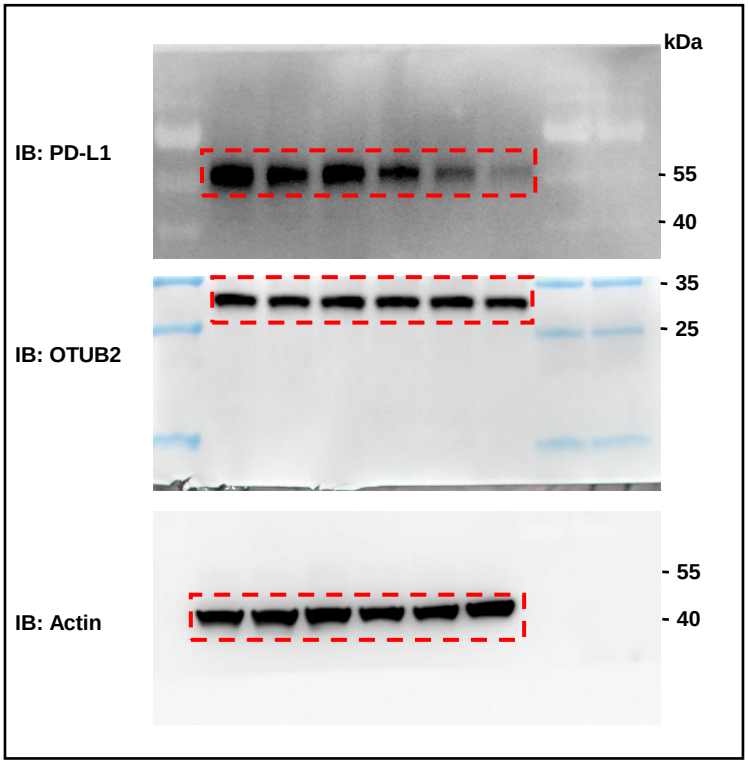

Uncropped blots for Supplementary Fig. 20b

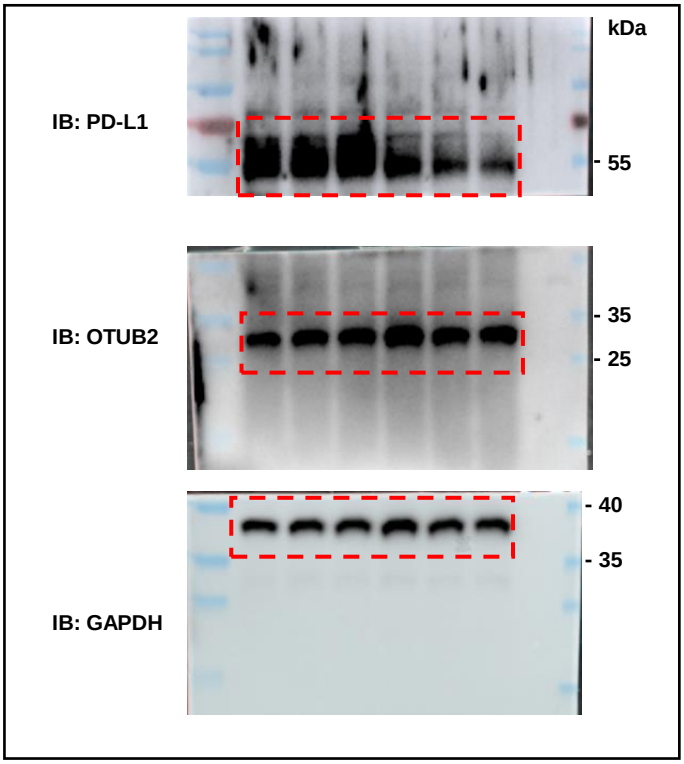

Uncropped blots for Supplementary Fig. 20c

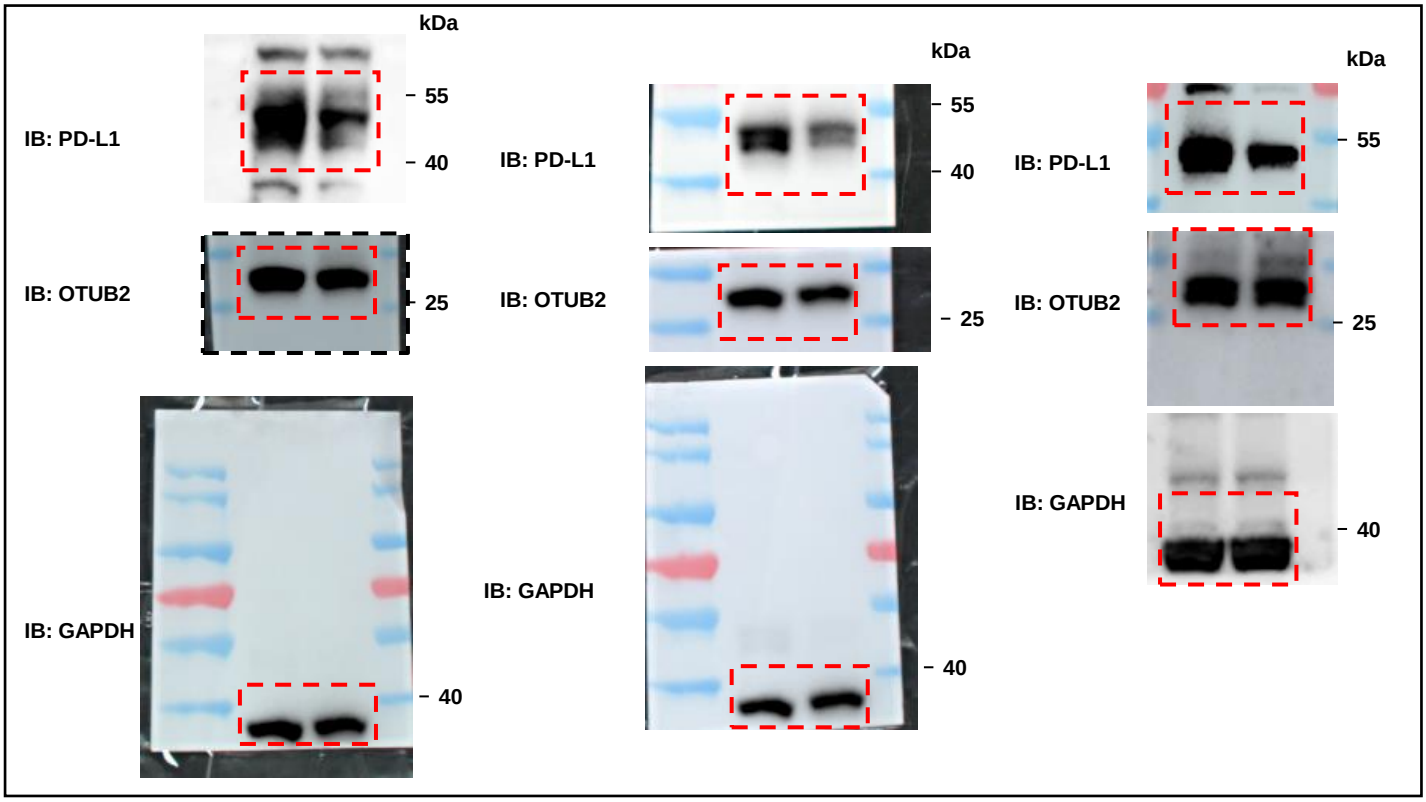

Uncropped blots for Supplementary Fig. 21